mathematics

MDPI

Article

Inverse Problem for an Extended Time-Dependent SEIRS Model: Validation with Real-World COVID-19 Data

Svetozar Margenov [1,2], Nedyu Popivanov [1,2,3], Tsvetan Hristov [3,*] and Veneta Koleva [3]

[1] Institute of Information and Communication Technologies, Bulgarian Academy of Sciences, 1113 Sofia, Bulgaria; margenov@parallel.bas.bg (S.M.); nedyu@parallel.bas.bg (N.P.)
[2] Centre of Excellence in Informatics and Information and Communication Technologies, 1113 Sofia, Bulgaria
[3] Faculty of Mathematics and Informatics, Sofia University "St. Kliment Ohridski", 1164 Sofia, Bulgaria; v.koleva@fmi.uni-sofia.bg
* Correspondence: tsvetan@fmi.uni-sofia.bg

Abstract

This paper introduces a novel SEIRS-type differential model that incorporates significant real-world factors such as vaccination, hospitalization, and vital dynamics. The model is described by a system of nonlinear ordinary differential equations with time-dependent parameters and coefficients. First, fundamental biological properties of the model, including the existence, uniqueness, and non-negativity of its solution, are established. In addition, using official COVID-19 data from Bulgaria, a special inverse problem for the differential model is formulated and investigated through the construction of an appropriate family of time-discrete inverse problems. As a result, the model parameters are identified, and the model is validated using real-world data. The presented numerical experiments confirm that the proposed methodology performs well in real-world applications with actual data. A very good agreement between computed and officially reported data with respect to the l_2 and l_∞ norms is obtained. The model and its simulation tools are adaptable and can be applied to datasets from other countries, provided suitable epidemiological data are available.

Keywords: COVID-19 pandemic; visualization; vaccination; hospitalization; vital dynamics; nonlinear ODEs; Cauchy problem; inverse problems; parameter identification; model validation

MSC: 34A34; 34C60; 65L05; 92C60

1. Introduction

The SARS-CoV-2 virus was first reported in December 2019 in Wuhan, Hubei Province, China, and its subsequent rapid global spread gave rise to the COVID-19 pandemic [1]. Despite the fact that various new vaccines have been developed and deployed since 2019, many countries have continued to experience epidemiological waves characterized by high infection and hospitalization rates. Nearly five years later, these challenges remain significant, and the virus continues to circulate. According to the World Health Organization (WHO) [2], as of 28 September 2025, a total of 778,741,840 COVID-19 cases had been reported, with the number of deaths globally reaching 7,102,636.

The spread of SARS-CoV-2 is typically modeled mathematically using either deterministic or stochastic approaches. Deterministic models assume a continuous host population, whereas stochastic models usually consider a discrete host population [3–6]. The stochastic

Check for updates

Academic Editor: Takashi Suzuki

Received: 25 November 2025
Revised: 14 December 2025
Accepted: 18 December 2025
Published: 20 December 2025

Copyright: © 2025 by the authors. Licensee MDPI, Basel, Switzerland. This article is an open access article distributed under the terms and conditions of the Creative Commons Attribution (CC BY) license.

approach allows for the capture of randomness and heterogeneity in disease transmission. In particular, it supports early-phase modeling for relatively smaller populations. Deterministic methods, however, offer important advantages in terms of transparency, interpretability, and computational efficiency. They scale very well to large populations and often perform better when forecasting overall pandemic trajectories. Moreover, their analytical tractability allows for the derivation of key epidemiological quantities such as the basic reproduction number, the herd-immunity threshold, and the timing of peak infectiousness.

Motivated by the proven capabilities of SIR-based frameworks and building on our own experience in advancing and refining their features, the present study focuses on the further development of this class of models.

To apply a deterministic model described by differential equations, one must know the time behavior of all involved parameters. In COVID-19 modeling, it is sometimes reasonable to assume that all parameters in certain models are known and even constant, although typically only for short periods of time [7–9]. However, when modeling the spread of a novel virus such as SARS-CoV-2, most of the parameters are initially unknown. This requires first solving an appropriate inverse problem to estimate the parameters from reported data. It is well known that inverse epidemiological problems involving nonlinear ordinary differential equations (ODEs) are generally ill-posed [10–12]. For this reason, it is necessary to determine parameters or combinations of parameters that can be uniquely identified from the available data. Typically, parameters are identified by solving an appropriate minimization problem [10,13–17]. For example, an extended SEIR model with hospitalization was studied in [10], and the corresponding inverse problem was reduced to the minimization of a quadratic objective functional. In [14], the parameter identification problem for a modified SEIR model was reduced to the minimization of a Tikhonov functional. In [15,16], the inverse problems for the classical nonlinear SIR and for an adaptive SIR model were solved by an iterative minimization procedure, resulting in well-posed linear systems. In the case of COVID-19, in particular, the inverse problems that arise from reported case data are nonstandard. Some functions and parameters in the model are known from empirical evidence, whereas the remaining functions and parameters must be determined. However, the compartment models used in COVID-19 modeling are typically extensions of the classical SIR model introduced by Kermack and McKendrick in [18]. The disruption of vaccination campaigns around the world necessitated the inclusion of a group representing vaccinated individuals in the models [19–22]. On the other hand, the limited capacity of hospitals and availability of intensive care unit (ICU) beds posed a serious challenge during the peak periods of the epidemic waves. Therefore, it was essential to employ models that account for hospital occupancy [23–27]. That is why, in our previous articles, we also introduced models with vaccination [28,29] and hospitalization [30]. Another important aspect of the COVID-19 pandemic, analyzed through deterministic models, is its impact on the economy, social life, and the progression of other diseases [31–35].

Let us mention also some results for the SEIR epidemic model for COVID-19 transmission using a Caputo derivative of fractional order [36–39].

In our previous paper [30], we studied a complex SEIRS-VBHC model in which hospitalized individuals are divided into two categories: non-critical and critical (requiring intensive care). Actually, the officially reported COVID-19 data are not enough to validate this model. Nevertheless, as we demonstrated in [30], it is possible to identify certain parameters within the SEIRS-VBHC model that are sufficient to compute both the basic and effective reproduction numbers.

Motivated by these limitations in real-world data availability, in this article, we present a unified framework for the mathematical analysis, modeling, computer simulation, and

visualization of the COVID-19 pandemic based on real epidemiological observations. This framework provides a consistent basis for the formulating inverse problems, estimating time-dependent epidemiological parameters, and validating the resulting models. In the present paper, we introduce a new SEIRS-VBH model in which hospitalized critical cases are not treated as a separate group for which we do not have enough information. This formulation enables the use of additional information on new hospital admissions (or the cumulative total number) to identify all model parameters and validate the model. More precisely, in Section 2, the SEIRS-VBH model is introduced, and the corresponding direct problem is stated. Special extended direct and inverse problems are formulated based on reported COVID-19 data in Bulgaria. The biologically reasonable mathematical properties of the model are established in Section 3. The practical identifiability of the model is discussed in Section 4. In Section 5, following the approaches described in [40,41], a special family of nonstandard semi-implicit variants of the model is proposed, and the biologically meaningful properties of the discrete variants are studied. The employed nonstandard schemes significantly improve the accuracy of the results. Furthermore, a family of time-discrete inverse problems is formulated, and a unique solving algorithmis developed. In Section 6, this algorithm is applied to the reported COVID-19 data in Bulgaria. Then, by numerically solving the direct differential problem, we identify the discrete inverse problem whose solution provides the best approximation of the reported data with respect to the $\{l_2\}$ and $\{l_\infty\}$ sub-norms. Section 7 presents the simulation tool developed by the authors of present paper for implementing the concept and algorithm outlined in Sections 5 and 6. A visualization of the results obtained from the model validation are presented in Appendix A. A discussion and conclusions are outlined in Section 8 and Section 9, respectively.

2. Differential Model SEIRS-VBH and Statement of the Inverse Problem

In order to study the transmission dynamics of the SARS-CoV-2 strain of coronavirus, we introduce a new deterministic SEIRS-VBH model with time-dependent parameters. Although developed for COVID-19, the model could potentially also be applied to the spread of other viral infections. According to the new model, the host population is divided into the following compartments: Susceptible (S), Exposed (E), Infectious (I), Recovered (R), Vaccinated Susceptible (V), Individuals with vaccination-acquired immunity (B), and Hospitalized (H). For clarity, we note that (V) is the group of individuals who have been vaccinated but remain susceptible to infection for a short period until antibodies develop, while (B) denotes the group of individuals who have developed antibodies as a result of vaccination and are therefore protected. The movement of individuals among the SEIRS-VBH model compartments is illustrated in Figure 1. As can be seen, the proposed model also incorporates vital dynamics and accounts for the loss of immunity in both vaccinated and recovered individuals.

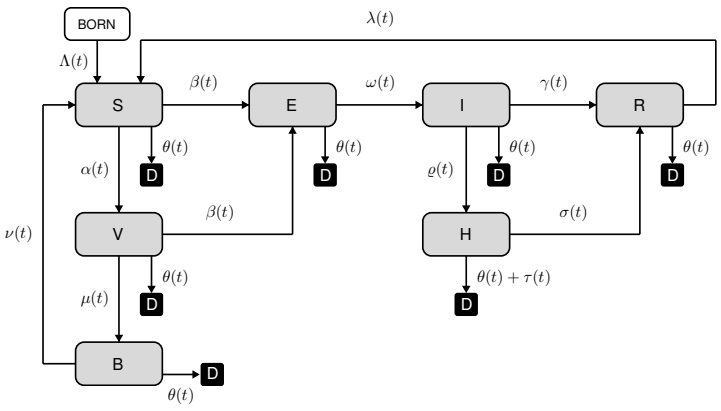


Figure 1. Transfer diagram of the SEIRS-VBH model.

The model is described mathematically by the following Cauchy problem for a system of nonlinear ordinary differential equations:

$$\begin{aligned}
\frac{dS}{dt} &= -\left[\alpha(t) + \theta(t) + \frac{\beta(t)}{N(t)} I(t)\right] S(t) + \Lambda(t)N(t) + \lambda(t)R(t) + \nu(t)B(t),\\
\frac{dE}{dt} &= -[\omega(t) + \theta(t)]E(t) + \frac{\beta(t)}{N(t)}[S(t) + V(t)]I(t),\\
\frac{dI}{dt} &= -[\gamma(t) + \rho(t) + \theta(t)]I(t) + \omega(t)E(t),\\
\frac{dR}{dt} &= -[\lambda(t) + \theta(t)]R(t) + \gamma(t)I(t) + \sigma(t)H(t),\\
\frac{dV}{dt} &= -\left[\mu(t) + \theta(t) + \frac{\beta(t)}{N(t)} I(t)\right] V(t) + \alpha(t)S(t),\\
\frac{dB}{dt} &= -[\nu(t) + \theta(t)]B(t) + \mu(t)V(t),\\
\frac{dH}{dt} &= -[\sigma(t) + \theta(t) + \tau(t)]H(t) + \rho(t)I(t),
\end{aligned} \tag{1}$$

with non-negative initial conditions of

$$S(t_0) = S_0, E(t_0) = E_0, I(t_0) = I_0, R(t_0) = R_0, V(t_0) = V_0, B(t_0) = B_0, H(t_0) = H_0. \tag{2}$$

Here,

$$N(t) := S(t) + E(t) + I(t) + R(t) + V(t) + B(t) + H(t)$$

is the total population size (the number of all living individuals), and $t_0 \geq 0$. The coefficients in the system (1) are time-dependent, and they involve the parameters listed in Table 1.

Table 1. Parameters of the SEIRS-VBH model.

Parameter	Description—Biological Meaning
$\alpha(t) = a(t)\varphi(t)$	Vaccination parameter
$a(t)$	Vaccination rate at moment t (number of vaccinated individuals/the entire population)
$\varphi(t)$	Vaccine effectiveness (excess risk/risk among vaccinated)
$\beta(t)$	Transmission rate—average number of adequate contacts (i.e., contacts sufficient for transmission) of a person at moment t
$\gamma(t)$	Recovery rate of non-hospitalized individuals (1/time for recovery)
$\varrho(t)$	Hospitalization rate at moment t (new hospitalized/infectious)
$\sigma(t)$	Recovery rate of hospitalized individuals (1/time for recovery)
$\tau(t)$	Mortality rate of infectious people at moment t (new deaths/infectious)
$\Lambda(t)$	Birth rate at moment t (new born/entire population)
$\theta(t)$	Natural mortality rate at moment t (new deaths/entire population)
$\lambda(t)$	Reinfection rate of recovered individuals (1/the duration of immune responses)
$\mu(t)$	Antibody rate (1/time taken for antibodies to develop)
$\nu(t)$	Reinfection rate of vaccinated individuals (1/the duration of immune responses)
$\omega(t)$	Latency rate (1/incubation period)

We call this deterministic problem the direct problem.

Direct problem: Suppose that the initial data, i.e.,

$$X_0 = (S_0, E_0, I_0, R_0, V_0, B_0, H_0)$$

and all parameters, i.e.,

$$p(t) = (\alpha(t), \beta(t), \gamma(t), \varrho(t), \sigma(t), \tau(t), \Lambda(t), \theta(t), \lambda(t), \mu(t), \nu(t), \omega(t)), \tag{3}$$

are known for $t \in [t_0, T]$. Solve the Cauchy problem (1), (2) and find the unknown function, i.e.,

$$X(t) = (S(t), E(t), I(t), R(t), V(t), B(t), H(t)), \tag{4}$$

for $t \in [t_0, T]$.

Unfortunately, in practice, the parameters are unknown, except a subset that can be determined based on statistical data. On the other hand, officially reported data provide information about certain functions in the model or about other functions closely related to the model. Thus, depending on the available data, various interesting inverse problems arise, some of which can be solved.

Official COVID-19 data are typically available for the following:

1. $A(t) = E(t) + I(t) + H(t)$—The number of active cases;
2. $Rtotal(t)$—The cumulative number of individuals who have recovered from the disease up to time t. In contrast to $R(t)$, this group includes individuals who have recovered but may have since lost their immunity acquired from the disease.
3. $Htotal(t)$—The cumulative number of individuals hospitalized due to the disease up to time t. Typically, the reported data are for new hospital admissions. Their sum up to time t corresponds to $Htotal(t)$.
4. $Dtotal(t)$—The cumulative number of COVID-19 deaths up to time t;
5. $Vtotal(t)$—The cumulative number of vaccinated individuals up to time t;

This allows us, similarly to the SIR-type models (see [7,28]), to expand the SEIRS-VBH model with the following linear equations:

$$\begin{aligned} \frac{dRtotal}{dt} &= \gamma(t)I(t) + \sigma(t)H(t), \\ \frac{dVtotal}{dt} &= a(t)N(t), \\ \frac{dHtotal}{dt} &= \rho(t)I(t), \\ \frac{dDtotal}{dt} &= \tau(t)H(t), \end{aligned} \tag{5}$$

with initial conditions of

$$Rtotal(t_0) = Rtotal_0, Vtotal(t_0) = Vtotal_0, Htotal(t_0) = Htotal_0, Dtotal(t_0) = Dtotal_0. \tag{6}$$

The $Rtotal$ equation in (5) represents the influx of newly recovered individuals originating both from the infectious population (captured by the $\gamma(t)I(t)$ term) and from the hospitalized compartment (represented by $\sigma(t)H(t)$). The $Vtotal$ equation in (5) accounts for the number of vaccinated individuals who have not yet acquired immunity and are susceptible to the disease. The $Htotal$ equation in (5) describes the dynamics of newly hospitalized cases, while the $Dtotal$ equation in (5) represents the flow of newly deceased individuals.

For convenience, we introduce the following notations for the functions:

$$m(t) := (A(t),\ H(t),\ Rtotal(t),\ Dtotal(t),\ Vtotal(t),\ Htotal(t)),$$

$$m_0 := (A(t_0),\ H(t_0),\ Rtotal(t_0),\ Dtotal(t_0),\ Vtotal(t_0),\ Htotal(t_0)).$$

Next, we formulate the following:

Extended direct problem: Suppose that the initial data, i.e., X_0, m_0, and all parameters, i.e., $p(t)$, are known for $t \in [t_0, T]$. Solve Cauchy problems (1), (2) and (5), (6) and find all functions ($X(t)$ and $m(t)$) for $t \in [t_0, T]$.

To formulate the appropriate inverse problem, we introduce the function expressed as

$$g(t) := (S(t),\ E(t),\ I(t),\ R(t),\ V(t),\ B(t)),$$

which represents quantities for which official data are typically unavailable and will therefore be treated as unknown. In contrast, the $m(t)$ function corresponds to quantities for which official data are generally available and will, thus, be considered to be known.

In the same manner, we divide the parameters ($p(t)$) into two separate groups: a group of known parameters, i.e.,

$$q(t) := (\Lambda(t), \theta(t), \lambda(t), \mu(t), \nu(t), \omega(t), \varphi(t)),$$

where we add vaccine effectiveness ($\varphi(t)$), and a group of unknown parameters, i.e.,

$$r(t) := (\alpha(t), \beta(t), \gamma(t), \varrho(t), \sigma(t), \tau(t)).$$

Finally, we formulate a special inverse problem corresponding to the extended direct problem described above.

Inverse Problem (P_{inv}): Let the initial data (X_0, m_0), the functions ($m(t)$), and the parameters ($q(t)$) be given on the interval of $[t_0, T]$. Then, using the system of differential Equation (1), find the functions ($g(t)$) and the parameters ($r(t)$) for $t \in [t_0, T]$.

Remark 1. *The required smoothness of the functions will be specified as needed in the corresponding context.*

Since the reported data provide the functions ($m(t)$) as piece-wise constant (step) functions of time, it is natural to also search for $g(t)$ and $r(t)$ as step functions. For this reason, we introduce a family of time-discrete variants of the SEIRS-VBH model and formulate an appropriate family of discrete variants (problems) of problem P_{inv}.

3. Mathematical Analysis of the Differential SEIRS-VBH Model

Let us consider the SEIRS-VBH model for the time frame of $[t_0, T]$, where $T > t_0$. In the traditional SIR and SEIR models [18], as well as in several SIR/SEIR-based models with fixed coefficients, it is assumed that the population size (N) remains constant. However, in model (1), the population size ($N(t)$) is a time-varying function.

Clearly, $N(t) > 0$ for all $t \in [t_0, T]$, as the total population size represents the sum of biologically meaningful and non-negative subpopulations (e.g., susceptible, exposed, infected, etc.). Moreover, from a biological perspective, $N(t)$ must remain strictly positive, since the model assumes an initially non-zero population (i.e., $N(t_0) > 0$).

Our first goal is to show that the proposed model possesses biologically reasonable properties. In particular, it has a unique solution that remains non-negative and is bounded

above by a function depending on the initial population size, as well as on the birth and mortality rates. Such boundedness guarantees the viability of the population.

To study the biologically meaningful properties of the model under the assumption of a fixed total population size (1), following [28,42], we introduce the following functions:

$$\begin{aligned} \tilde{S}(t) &:= \frac{S(t)}{N(t)}, \tilde{E}(t) := \frac{E(t)}{N(t)}, \tilde{I}(t) := \frac{I(t)}{N(t)}, \tilde{R}(t) := \frac{R(t)}{N(t)} \\ \tilde{V}(t) &:= \frac{V(t)}{N(t)}, \tilde{B}(t) := \frac{B(t)}{N(t)}, \tilde{H}(t) := \frac{H(t)}{N(t)}. \end{aligned} \tag{7}$$

For the new unknown functions, using (1) and (2), we obtain the following reduced Cauchy problem:

$$\begin{aligned} \frac{d\tilde{S}}{dt} &= -\left[\alpha(t) + \beta(t)\tilde{I}(t) + \Lambda(t) - \tau\tilde{H}(t)\right]\tilde{S}(t) + \Lambda(t) + \lambda(t)\tilde{R}(t) + \nu(t)\tilde{B}(t), \\ \frac{d\tilde{E}}{dt} &= -\left[\omega(t) + \Lambda(t) - \tau(t)\tilde{H}(t)\right]\tilde{E}(t) + \beta(t)\left[\tilde{S}(t) + \tilde{V}(t)\right]\tilde{I}(t), \\ \frac{d\tilde{I}}{dt} &= -\left[\gamma(t) + \varrho(t) + \Lambda(t) - \tau(t)\tilde{H}(t)\right]\tilde{I}(t) + \omega(t)\tilde{E}(t), \\ \frac{d\tilde{R}}{dt} &= -\left[\lambda(t) + \Lambda(t) - \tau(t)\tilde{H}(t)\right]\tilde{R}(t) + \gamma(t)\tilde{I}(t) + \sigma(t)\tilde{H}(t), \\ \frac{d\tilde{V}}{dt} &= -\left[\mu(t) + \beta(t)\tilde{I}(t) + \Lambda(t) - \tau(t)\tilde{H}(t)\right]\tilde{V}(t) + \alpha(t)\tilde{S}(t), \\ \frac{d\tilde{B}}{dt} &= -\left[\nu(t) + \Lambda(t) - \tau(t)\tilde{H}(t)\right]\tilde{B}(t) + \mu(t)\tilde{V}(t), \\ \frac{d\tilde{H}}{dt} &= -[\sigma(t) + \tau(t) + \Lambda(t)]\tilde{H}(t) + \tau(t)\tilde{H}^2(t) + \varrho(t)\tilde{I}(t), \end{aligned} \tag{8}$$

with non-negative initial conditions of

$$\tilde{S}(t_0) = \tilde{S}_0, \tilde{E}(t_0) = \tilde{E}_0, \tilde{I}(t_0) = \tilde{I}_0, \tilde{R}(t_0) = \tilde{R}_0, \tilde{V}(t_0) = \tilde{V}_0, \tilde{B}(t_0) = \tilde{B}_0, \tilde{H}(t_0) = \tilde{H}_0, \tag{9}$$

where $(\tilde{S}_0, \tilde{E}_0, \tilde{I}_0, \tilde{R}_0, \tilde{V}_0, \tilde{B}_0, \tilde{H}_0) = (S_0, E_0, I_0, R_0, V_0, B_0, H_0)/N(t_0)$.

Subsequently, let us introduce the following notations:

$$\begin{aligned} \tilde{X}(t) &:= \left(\tilde{S}(t), \tilde{E}(t), \tilde{I}(t), \tilde{R}(t), \tilde{V}(t), \tilde{B}(t), \tilde{H}(t)\right), \\ \tilde{N}(t) &:= \tilde{S}(t) + \tilde{E}(t) + \tilde{I}(t) + \tilde{R}(t) + \tilde{V}(t) + \tilde{B}(t) + \tilde{H}(t), \\ \tilde{X}_0 &:= (\tilde{S}_0, \tilde{E}_0, \tilde{I}_0, \tilde{R}_0, \tilde{V}_0, \tilde{B}_0, \tilde{H}_0), \\ \tilde{N}_0 &:= \tilde{S}_0 + \tilde{E}_0 + \tilde{I}_0 + \tilde{R}_0 + \tilde{V}_0 + \tilde{B}_0 + \tilde{H}_0. \end{aligned} \tag{10}$$

It is clear that if problem (8), (9) is obtained from problem (1), (2) by the substitution of (7), then $\tilde{N}(t) = 1$ for $t \in [t_0, T]$. However, if we consider Cauchy problem (8), (9) as a problem independent of Cauchy problem (1), (2), then the property of $\tilde{N}(t) = 1$ does not necessarily hold, and the following lemma is particularly useful.

Lemma 1. *Let $p(t) \in C([t_0, T^*])$ for some $T^* \in (t_0, T]$ and the initial data $(\tilde{X}_0)$ satisfy the condition of $\tilde{N}_0 = 1$. Suppose that there exists a solution $(\tilde{X} \in C^1([t_0, T^*]))$ of Cauchy problem (8), (9). Then , for the sum of the components of $\tilde{X}(t)$, we have $\tilde{N}(t) = 1$ for all $t \in [t_0, T^*]$.*

Proof. By summing up all equations in system (8), we find that $\tilde{N}(t)$ satisfies the following first-order linear ordinary differential equation and the initial condition of $\tilde{N}(t_0) = 1$:

$$\frac{d\tilde{N}}{dt} = -\left(\Lambda(t) + \tau(t)\tilde{H}(t)\right)\tilde{N}(t) + \Lambda(t) + \tau(t)\tilde{H}(t) \tag{11}$$

Obviously, $\tilde{N}(t) \equiv 1$ is a solution of the obtained Cauchy problem. We also note that this Cauchy problem has a unique solution, since the coefficients in Equation (11) are continuous for $t \in [t_0, T^*]$.

The proof is complete. □

Remark 2. *According to the notation used here and throughout, we say that a real vector* $(x = (x_1, x_2, \ldots, x_n))$ *is* non-negative (positive) *if all its components* (x_j) *are non-negative (positive). Furthermore, we use the* l_1 *norm defined as* $\|x\|_1 = |x_1| + |x_2| + \cdots + |x_n|$. *Actually, for* $x \geq 0$, *the norm is* $\|x\|_1 = x_1 + x_2 + \cdots + x_n$.

Furthermore, we study Cauchy problem (8), (9), as we are focused on a real-world epidemic scenario in which, at the initial time, the numbers of susceptible individuals $(\tilde{S}(t_0))$ and infectious individuals $(\tilde{I}(t_0))$ are both positive. For this purpose, we introduce the following set:

$$\tilde{\Sigma} := \left\{\tilde{X} = (\tilde{S}, \tilde{E}, \tilde{I}, \tilde{R}, \tilde{V}, \tilde{B}, \tilde{H}) : \tilde{X} \geq 0, \tilde{S} > 0, \tilde{I} > 0, \|\tilde{X}\|_1 = 1\right\}. \tag{12}$$

We now prove the following existence and uniqueness theorem, in which neither the condition of $\tilde{H}_0 > 0$ nor the restriction to $H(t) > 0$ imposed in Theorem 1 in [30] is required.

Theorem 1. *Let* $\tilde{X}_0 \in \tilde{\Sigma}$, $p(t) \in C([t_0, T])$, *and* $p(t) \geq 0$ *for* $t_0 \leq t \leq T$. *Then, there exists a unique solution* $(\tilde{X}(t))$ *of Cauchy problem* (8), (9), *which is well-defined and bounded for all* $t \in [t_0, T]$. *In addition,* $\tilde{X}(t) \in \tilde{\Sigma}$ *for* $t \in [t_0, T]$.

Proof. Owing to the specific structure of the vector-valued function appearing on the right-hand side of system (8) (whose components are second-order polynomials with respect to $\tilde{X}$ components), this function is continuous and differentiable. Then, according to Picard's existence and uniqueness theorem (Theorem 1.1., p. 8 in [43] or Theorem 2., p. 20 in [44]), there exists a unique solution $(\tilde{X}(t))$ of Cauchy problem (8) with initial conditions (9) defined in the interval of $[t_0, T_1]$ for some $T_1 \in (t_0, T]$.

Our next goal is to prove that $T_1 = T$.

Step 1. Here, we prove that $\tilde{X}(t) \geq 0$ and $\tilde{S}(t) > 0$, $\tilde{I}(t) > 0$ for $t \in [t_0, T_1]$.

Let us consider the $\tilde{S}$-th, the $\tilde{E}$-th, the $\tilde{I}$-th, the $\tilde{R}$-th, the $\tilde{V}$-th, and the $\tilde{B}$-th equation from system (8). All these equations are linear first-order differential equations in the form of

$$\frac{d\tilde{x}}{dt} = P(t)\tilde{x}(t) + Q(t), \tag{13}$$

where $P(t)$ and $Q(t)$ are continuous functions over the interval of $[t_0, T_1]$. The unique solution to the Cauchy problem for Equation (13) with an initial condition of

$$\tilde{x}(t_0) = \tilde{x}_0 \tag{14}$$

is given by the following formula:

$$\tilde{x}(t) = \exp\left(-\int_{t_0}^{t} P(s)ds\right)\left[\tilde{x}_0 + \int_{t_0}^{t} Q(s)\exp\left(\int_{t_0}^{s} P(u)\,du\right)ds\right],\ t_0 \leq t \leq T_1. \tag{15}$$

From (15), it is then obvious that if $\tilde{x}_0 \geq 0$ and $Q(s) \geq 0$ over the interval of integration $[t_0, t]$, then $\tilde{x}(t) \geq 0$ at all points $t \in [t_0, T_1]$. If, in addition, $\tilde{x}_0 > 0$, then $\tilde{x}(t) > 0$.

Now, taking into account $\tilde{I}(t_0)\tilde{S}(t_0) > 0$, we assume that $\tilde{S}(t)\tilde{I}(t)$ vanishes at some points in $(t_0, T_1]$. Let $t_1 \in (t_0, T_1]$ denote the first time such that $\tilde{S}(t_1)\tilde{I}(t_1) = 0$. Then,

(i) The $\tilde{V}$ equation of system (8) is in the form of (13), and we can use (15) with $\tilde{x}_0 = V_0 \geq 0$ and $Q(s) = \alpha(s)\tilde{S}(s) \geq 0$ in $[t_0, t_1]$. Therefore, $\tilde{V}(t) \geq 0$ throughout the interval of $[t_0, t_1]$.

(ii) The $\tilde{B}$ equation of system (8) is in the form of (13), with $\tilde{x}_0 = B_0 \geq 0$ and $Q(s) = \mu(s)\tilde{V}(s) \geq 0$ in $[t_0, t_1]$. Hence, $\tilde{B}(t) \geq 0$ for $t \in [t_0, t_1]$.

(iii) The $\tilde{E}$ equation of system (8) is in the form of (13), with $\tilde{x}_0 = E_0 \geq 0$ and $Q(s) = \beta(s)\left[\tilde{S}(s) + \tilde{V}(s)\right]\tilde{I}(s) \geq 0$ in $[t_0, t_1]$. It follows that $\tilde{E}(t) \geq 0$ for $t \in [t_0, t_1]$.

(iv) The $\tilde{I}$ equation from system (8) conforms to the form of (13), with $\tilde{x}_0 = \tilde{I}_0 > 0$ and $Q(s) = \omega(s)\tilde{E}(s) \geq 0$ in $[t_0, t_1]$. Therefore, $\tilde{I}(t_1) > 0$.

(v) The $\tilde{H}$ equation from system (8) is not in the form of (13), but it is a Riccati equation with respect to $\tilde{H}$. Taking into account $\tilde{H}(t_0) \geq 0$, we assume there exists a point ($t_2 \in (t_0, t_1]$) such that $\tilde{H}(t_2) < 0$. Then, since $\tilde{H}(t)$ is a continuous function on $[t_0, t_1]$, there exists a point ($t^* \in [t_0, t_2)$) such that $\tilde{H}(t^*) = 0$ and $\tilde{H}(t) < 0$ for all $t \in (t^*, t_2]$. Then, the $\tilde{H}$ equation from system (8) gives

$$\frac{d\tilde{H}}{dt}(t) = -[\sigma(t) + \tau(t) + \Lambda(t)]\tilde{H}(t) + \tau(t)\tilde{H}^2(t) + \varrho(t)\tilde{I}(t) \geq 0$$

for $t \in [t^*, t_2]$. This leads to a contradiction with $\tilde{H}(t^*) = 0$ and $\tilde{H}(t) < 0$ for $t \in (t^*, t_2]$. Therefore, $\tilde{H}(t) \geq 0$ for $t \in [t_0, t_1]$.

(vi) The $\tilde{R}$ equation from system (8) conforms to the form of (13), with $\tilde{x}_0 = \tilde{R}_0 \geq 0$ and $Q(s) = \gamma(s)\tilde{I}(s) + \sigma(s)\tilde{H}(s) \geq 0$ in $[t_0, t_1]$. Therefore, $\tilde{R}(t) \geq 0$ for $t \in [t_0, t_1]$.

(vii) Now, since the $\tilde{S}$ equation from system (8) conforms to the form of (13) with $\tilde{x}_0 = \tilde{S}_0 > 0$ and $Q(s) = \Lambda(s) + \lambda(s)\tilde{R}(s) + \nu(s)\tilde{B}(s) \geq 0$ in $[t_0, t_1]$, it follows that $\tilde{S}(t_1) > 0$.

The results in (iv) and (vii) lead to a contradiction with $\tilde{S}(t_1)\tilde{I}(t_1) = 0$. Hence, it follows that $S(t) > 0$ and $I(t) > 0$ for $t \in [t_0, T_1]$.

Now, it easy to repeat stages (i), (ii), (iii), (v), and (vi) on the interval of $[t_0, T_1]$ instead of $[t_0, t_1]$ and conclude that $\tilde{X}(t) \geq 0$ for $t \in [t_0, T_1]$.

Step 2. Since $p(t) \in C([t_0, T_1])$ and $\tilde{X}(t) \in C^1([t_0, T_1])$ is a solution of Cauchy problem (8), (9) with $\tilde{X}(t) \geq 0$, $\tilde{S}(t) > 0$, $\tilde{I}(t) > 0$ in $[t_0, T_1]$ and $\|\tilde{X}(t_0)\|_1 = 1$, Lemma 1 gives $\|\tilde{X}(t)\|_1 = 1$ for all $t \in [t_0, T_1]$. Therefore, the solution is $\tilde{X}(t) \in \tilde{\Sigma}$ for $[t_0, T_1]$, and it is uniformly bounded on $[t_0, T_1]$. According to the Extension Theorem (Theorem 3.1, p. 12 in [43] or Proposition (A), p. 189 in [44]), it follows that $T_1 = T$, which means solution $\tilde{X}(t)$ exists on the interval of $[t_0, T]$ and $\tilde{X}(t) \in \tilde{\Sigma}$ for $t \in [t_0, T]$.

This completes the proof. □

In order to study the original Cauchy problem (1), (2) for $t \in [t_0, T]$, we introduce the following sets:

$$\Sigma(t) := \Big\{ X(t) = (S(t), E(t), I(t), R(t), V(t), B(t), H(t)) : X(t) \geq 0, S(t) > 0,$$
$$I(t) > 0, \|X(t)\|_1 \leq N_0 \exp\left(\int_{t_0}^{t} [\Lambda(s) - \theta(s)]\, ds \right) \Big\},$$

where $N_0 = \|X_0\|_1$.

We are now prepared to formulate the following existence and uniqueness theorem, which also provides an upper bound for the population size ($N(t)$).

Theorem 2. *Let the initial data be $X_0 \in \Sigma(t_0)$, $p \in C([t_0, T])$ and $p(t) \geq 0$ for $t_0 \leq t \leq T$. Then, there exists a solution $(X(t))$ of Cauchy problem (1) and (2), which is defined for $t \in [t_0, T]$, and $X(t) \in \Sigma(t)$ for $t \in [t_0, T]$. The solution with such properties is unique.*

Proof. To prove the existence and uniqueness of such a solution, we use Theorem 1.

(i) **Existence.**
As $X_0 \geq 0$ with $S_0 > 0$ and $I_0 > 0$, let us consider Cauchy problem (8), (9) with an initial condition of $\tilde{X}_0 := X_0/N_0 \geq 0$. Since $\tilde{S}_0 = S_0/N_0 > 0$ and $\tilde{I}_0 = I_0/N_0 > 0$ are both strictly positive, $\|\tilde{X}_0\|_1 = 1$ and all other conditions required by Theorem 1 are satisfied, it follows that Theorem 1 guarantees the existence of a function $(\tilde{X}(t) = \left(\tilde{S}(t), \tilde{E}(t), \tilde{I}(t), \tilde{R}(t), \tilde{V}(t), \tilde{B}(t), \tilde{H}(t)\right) \in \tilde{\Sigma},)$ that is a unique solution of problem (8), (9) defined for $t \in [t_0, T]$.
Next, we consider the following Cauchy problem:

$$\begin{aligned} \frac{dN}{dt} &= \left[\Lambda(t) - \theta(t) - \tau(t)\tilde{H}(t)\right]N(t), \\ N(t_0) &= N_0. \end{aligned} \tag{16}$$

It follows directly that the unique solution to problem (16) is

$$N(t) = N_0 \exp\left(\int_{t_0}^{t} \left[\Lambda(s) - \theta(s) - \tau(s)\tilde{H}(s)\right] ds\right) > 0$$

and is defined for $t \in [t_0, T]$.
As shown earlier, system (1) can be transformed into (8). Now, by reversing this transformation using $N(t) > 0$, we find that the function expressed as $X(t) := N(t)\tilde{X}(t) \geq 0$ is a solution to the Cauchy problem defined by (1), (2) on the interval of $[t_0, T]$ and satisfies $S(t) > 0$ and $I(t) > 0$ for all $t \in [t_0, T]$.
Furthermore, by summing up all equations in system (1) and the initial conditions (2), we derive the following Cauchy problem:

$$\begin{aligned} \frac{dN}{dt} &= [\Lambda(t) - \theta(t)]N(t) - \tau(t)H(t), \\ N(t_0) &= N_0, \end{aligned} \tag{17}$$

which is, in fact, problem (16) with $\tilde{H}(t) = H(t)/N(t)$.
Problem (17) has a unique solution, i.e.,

$$N(t) = \exp\left(\int_{t_0}^{t} [\Lambda(s) - \theta(s)]\, ds\right)\left[N_0 - \int_{t_0}^{t} \tau(s)H(s) \exp\left(\int_{t_0}^{s} [\theta(u) - \Lambda(u)]\, du\right) ds\right].$$

Since $\tau(s)H(s) \geq 0$ in $[t_0, T]$, it follows that

$$N(t) \leq N_0 \exp\left(\int_{t_0}^{t} [\Lambda(s) - \theta(s)]\, ds\right).$$

Therefore, $X(t) \in \Sigma(t)$ for $t \in [t_0, T]$.

(ii) **Uniqueness.** The uniqueness of the solution is proven in a manner analogous to that used in Theorem 2 [28].

The proof is complete. □

4. Identifiability of the SEIRS-VBH Model

Mathematical models in epidemiology consist of many different coefficients (for example, see ODE system (1)). We are now attempting to solve ODE system (1) with the given initial conditions (2) in a case where all coefficients (epidemiological parameters) in system (1) are known. As usual, we refer to this as the **direct problem**. In contrast to the direct problem, we now seek to determine some unknown coefficients using additional information about the groups in solution $X(t)$. With this information at hand, it is possible to find the coefficients, which means that we solve a problem opposite to the direct problem (the so-called **inverse problem**). Such inverse problems arise in many practical situations (see [45,46] and references therein). These inverse problems are sometimes **ill-posed** in the sense of Hadamard, and in the current situation, we actually encounter such a case. More information about this procedure for solving epidemiological problems can be found in [46]. Each such problem requires a specific research approach.

In the present paper, we develop a methodology for approximating the reported COVID-19 data (five series of data points: active, recovered, vaccinated, hospitalized, and deceased cases) for Bulgaria using the differential SEIRS-VBH model. Here, we note that we are looking only for biologically reasonable values. As explained above, we first identify the parameters in the model by solving the **inverse problem** corresponding to the direct problem (1), (2). A criterion for assessing how well the parameters of the differential model are estimated from the reported data is the quality of the approximation. To measure approximation accuracy, we use relative errors with respect to the l_2 and l_∞ norms. We perform a perturbation analysis (using both ξ and c parameters) and find that the best approximation of the reported data with respect to the l_2 norm coincides with that obtained using the l_∞ norm. Moreover, the results presented in Figures 2 and 3 show very good agreement between the corresponding error margins of the l_2 and l_∞ norms. These observations suggest the robustness of the proposed SEIRS-VBH model with respect to the norm of choice within the $\{l_p\}$ family.

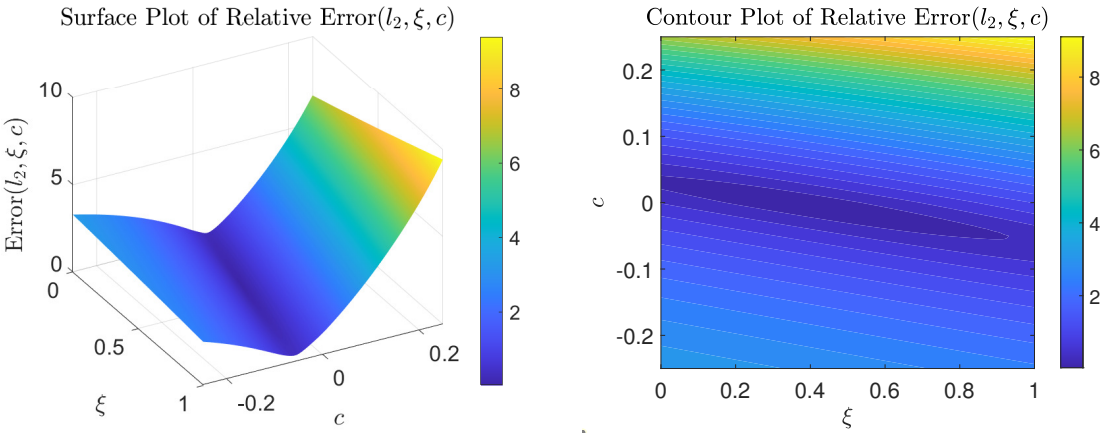


Figure 2. Surface and contour plots of relative error ($Error(l_2, \xi, c)$).

The available data for Bulgaria lead to a special **inverse problem**. To describe this complex situation more precisely and clearly, we provide a brief overview of the developed methodology:

1. We construct a family of discrete inverse problems that are uniquely solvable (see the Unique Solving Algorithm in Section 5). This is achieved by using a family of discrete variants of the differential model that involve two new parameters (ξ and c; see the difference scheme (20) and the function (40)).

2. We perturb the ξ and c parameters, and for each pair (ξ, c), we solve the corresponding discrete inverse problem (see Step 1 in Section 6). In this way, for each (ξ, c), we find a set of model parameters $(\alpha, \beta, \gamma, \varrho, \sigma, \tau)$. Each parameter set is specific to both the particular reported data and the corresponding discrete model.
3. We numerically solve the extended **direct problems** (1), (2) and (5), (6) using each of the identified parameter sets. These computations are performed using the ode45 solver in Matlab R2024a, which implements the Runge–Kutta 4th/5th-order method. As a result, we obtain numerical solutions (with a step of 0.01) of the original SEIRS-VBH model (see Step 2 in Section 6).
4. For each pair (ξ, c), we compute the corresponding relative approximation error with respect to the l_2 and l_∞ norms (see Step 3 in Section 6).
5. The minimum of the computed relative errors shows the best approximation of the official data with respect to the chosen error measure (see Step 4 in Section 6). This serves as our criterion for solving both the inverse and direct problems (for comparison, see Figures 4 and 5 and Appendix A.1).
6. In such a way, we fix the model parameters and all model curves, including those for the active, recovered, vaccinated, hospitalized, and deceased cases.

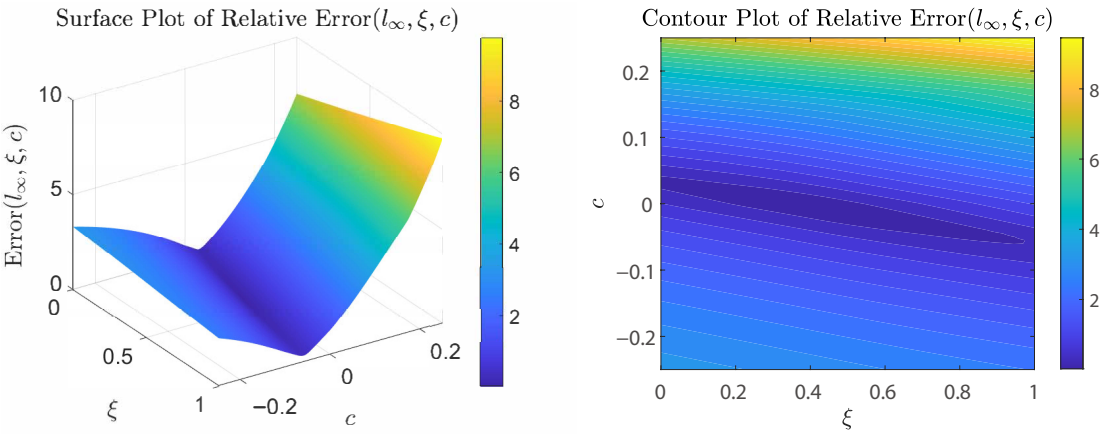


Figure 3. Surface and contour plots of relative error ($Error(l_\infty, \xi, c)$).

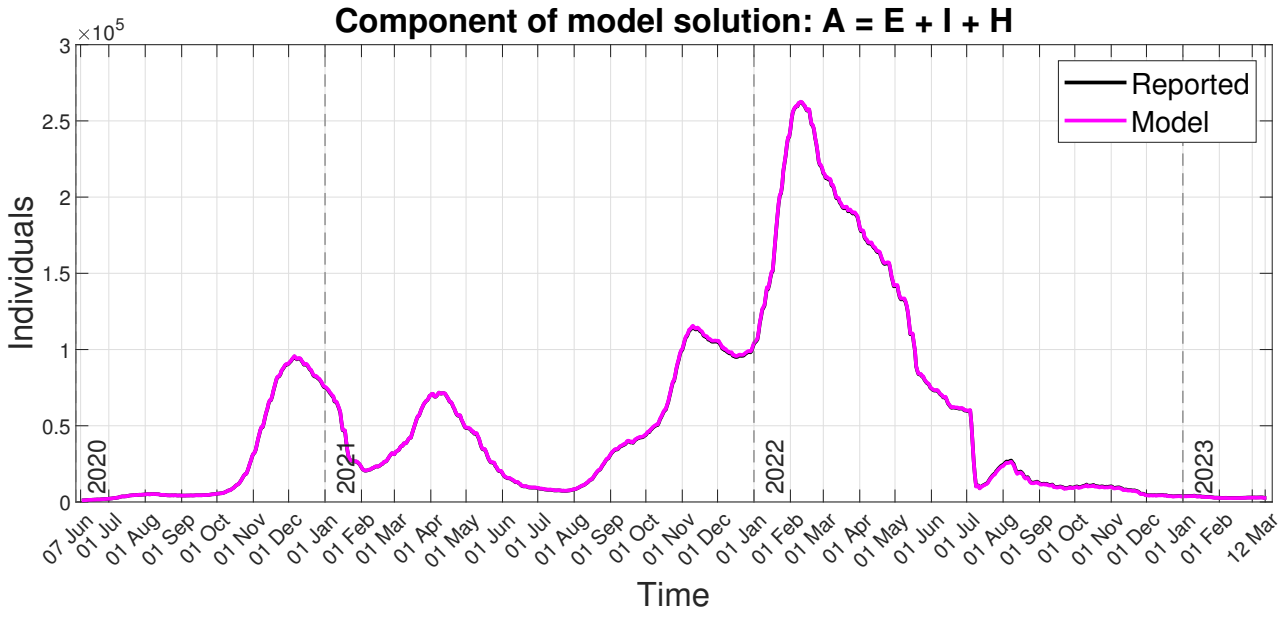


Figure 4. Reported data ($A_{reported}$) and model curve ($A_{computed}(\xi^*, c^*)$) of active cases.

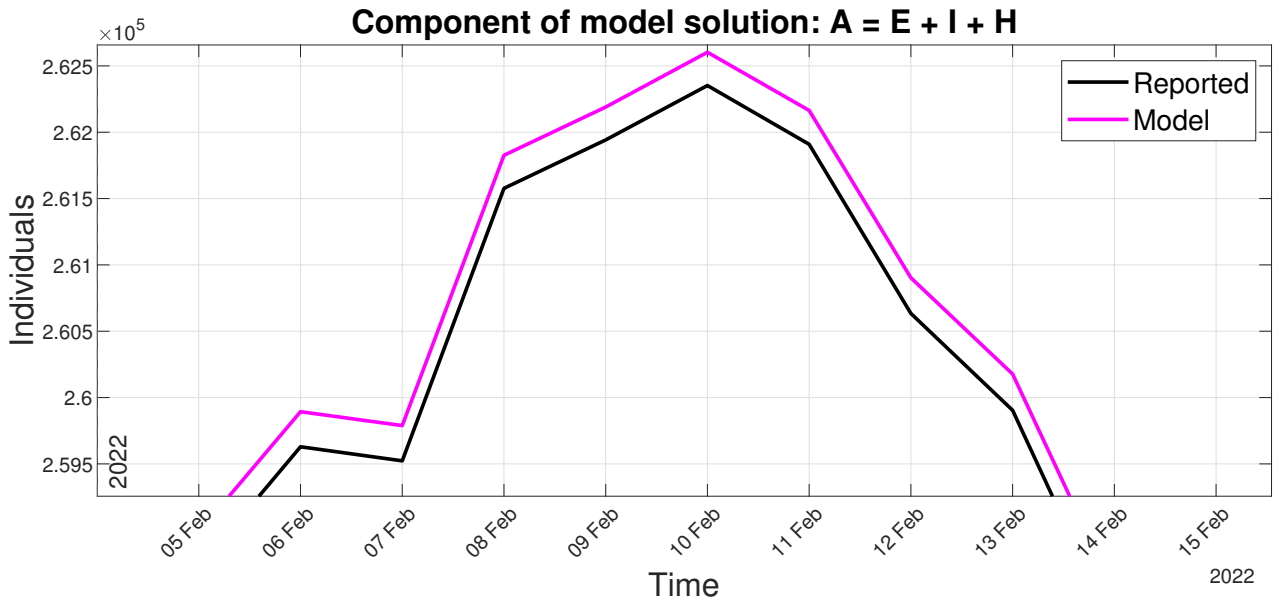


Figure 5. Reported data ($A_{reported}$) and model curve ($A_{computed}(\xi^*, c^*)$) of active cases for the period of 6–13 February 2022.

5. Discrete Variants of the Differential SEIRS-VBH Model and Related Discrete Inverse Problems

Let us note, again, that inverse epidemiological problems involving nonlinear ordinary differential equations are generally ill-posed.

Now, in order to formulate an appropriate family of discrete inverse problems related to the differential inverse problem P_{inv}, we introduce a family of discrete variants of the differential problem (1), (2), extended by (5), (6).

Let us consider a time frame of $t_1, t_2, \ldots, t_K \subseteqq [t_0, T]$, where $t_k = t_1 + (k-1)h$, $k = 2, 3, \ldots, K$ and a step size of $h > 0$. If $h = 1$ *day*, then t_k represents fixed consecutive days of the epidemic (actually, the official data for COVID-19 are reported once per day). Next, we introduce the notation for the values of functions in the model for $k = 1, 2, \ldots, K$, i.e.,

$$\begin{aligned} X_k &:= (S_k,\, E_k,\, I_k,\, R_k,\, V_k,\, B_k,\, H_k) \\ &= (S(t_k),\, E(t_k),\, I(t_k),\, R(t_k),\, V(t_k),\, B(t_k),\, H(t_k),), \end{aligned}$$

$$N_k := N(t_k) = S_k + E_k + I_k + R_k + V_k + B_k + H_k, \tag{18}$$

as well as the values of the parameters:

$$\begin{aligned} p_k &:= (\alpha_k,\, \beta_k,\, \gamma_k,\, \tau_k,\, \Lambda_k,\, \theta_k,\, \omega_k,\, \lambda_k,\, \mu_k,\, \nu_k,\, \varrho_k,\, \sigma_k) \\ &= (\alpha(t_k),\, \beta(t_k),\, \gamma(t_k),\, \tau(t_k),\, \Lambda(t_k),\, \theta(t_k),\, \omega(t_k),\, \lambda(t_k),\, \mu(t_k),\, \nu(t_k), \\ &\varrho(t_k),\, \sigma(t_k)), \end{aligned} \tag{19}$$

$k = 1, 2, \ldots, K-1$.

Remark 3. *Furthermore, each parameter value (p_{k-1}) is hereinafter considered the value corresponding to day t_k required to obtain X_k from X_{k-1}.*

Here, we propose time-discrete analogs of the differential SEIRS-VBH model. More precisely, for $0 < h \leq 1$, we introduce the following family of modified semi-implicit difference schemes with a weight of $\xi \in [0, 1]$ and a non-negative function ($\psi(h)$) that substitutes the step size (h) such that $\psi(h) = h + O(h^2)$ as $h \to +0$:

$$\begin{aligned}
\frac{S_k - S_{k-1}}{\psi(h)} &= -\left[\alpha_{k-1} + \theta_{k-1} + \frac{\beta_{k-1}}{N_{k-1}}(\xi I_{k-1} + (1-\xi) I_k)\right] S_{k-1} + \Lambda_{k-1} N_{k-1} \\
&\quad + \lambda_{k-1} R_{k-1} + \nu_{k-1} B_{k-1}, \\
\frac{E_k - E_{k-1}}{\psi(h)} &= -(\omega_{k-1} + \theta_{k-1}) E_{k-1} + \frac{\beta_{k-1}}{N_{k-1}}(S_{k-1} + V_{k-1})(\xi I_{k-1} + (1-\xi) I_k), \\
\frac{I_k - I_{k-1}}{\psi(h)} &= -(\gamma_{k-1} + \varrho_{k-1})(\xi I_{k-1} + (1-\xi) I_k) - \theta_{k-1} I_{k-1} + \omega_{k-1} E_{k-1}, \\
\frac{R_k - R_{k-1}}{\psi(h)} &= -(\lambda_{k-1} + \theta_{k-1}) R_{k-1} + \gamma_{k-1}(\xi I_{k-1} + (1-\xi) I_k) + \sigma_{k-1} H_{k-1}, \\
\frac{V_k - V_{k-1}}{\psi(h)} &= -\left[\mu_{k-1} + \theta_{k-1} + \frac{\beta_{k-1}}{N_{k-1}}(\xi I_{k-1} + (1-\xi) I_k)\right] V_{k-1} + \alpha_{k-1} S_{k-1}, \\
\frac{B_k - B_{k-1}}{\psi(h)} &= -(\nu_{k-1} + \theta_{k-1}) B_{k-1} + \mu_{k-1} V_{k-1}, \\
\frac{H_k - H_{k-1}}{\psi(h)} &= -(\sigma_{k-1} + \tau_{k-1} + \theta_{k-1}) H_{k-1} + \varrho_{k-1}(\xi I_{k-1} + (1-\xi) I_k),
\end{aligned} \tag{20}$$

where $k = 2, 3, \ldots, K$ and the initial values are $S_1 = S(t_1)$, $E_1 = E(t_1)$, $I_1 = I(t_1)$, $R_1 = R(t_1)$, $V_1 = V(t_1)$, $B_1 = B(t_1)$, $H_1 = H(t_1)$.

Remark 4. *In [40,41], a similar modified difference scheme was investigated but in the context of the classical SIR model. The proposed functions are* $\psi(h) = \exp(h) - 1$, $\psi(h) = 1 - \exp(-h)$, $\psi(h) = \sin(h)$. *In this study, we find and use different functions that yield better results for day* $h = 1$ *(which corresponds to the reported data). Since we apply the discrete model (20) with a step of day* $h = 1$, *only the value of* $\psi(1)$ *is relevant. Therefore, in the numerical experiments, we use specific simple functions, which will be defined later. Our goal is to construct an appropriate function* $(\psi(h))$ *that reduces the relative error of the computations.*

Our first objective is to show that the modified discrete problem (20), when provided with appropriate initial data, exhibits biologically plausible behavior comparable to that of the differential SEIRS-VBH model. Consequently, the next step involves determining sufficient conditions on the parameter values (p_k) given by (19) and the $\psi(h)$ function in the difference scheme (20) to ensure the component-wise non-negativity of the numerical solution.

Theorem 3. *Let* $h > 0$ *and* $\psi(h) > 0$ *be fixed and* $X_1 \geq 0$ *with* $S_1 > 0$, $I_1 > 0$, $p_{k-1} \geq 0$ *for all* $k = 2, 3, \ldots, K$. *Let the condition of*

$$\max_{k=2,\ldots,K} q_{k-1} < \frac{1}{\psi(h)} \tag{21}$$

with

$$\begin{aligned}
q_{k-1} :=& \theta_{k-1} + \max\Big\{\alpha_{k-1} + \beta_{k-1}, \omega_{k-1}, \mu_{k-1} + \beta_{k-1}, \gamma_{k-1} + \rho_{k-1}, \\
& \nu_{k-1}, \sigma_{k-1} + \tau_{k-1}, \lambda_{k-1}\Big\}
\end{aligned}$$

hold.

Then, for the values of $X_k = (S_k, E_k, I_k, R_k, V_k, B_k, H_k)$ *obtained from (20), we find that* $X_k \geq 0$ *with* $S_k > 0$, $I_k > 0$ *for* $k = 2, 3, \ldots, K$, *and the estimate of*

$$N_k \leq N_1 \prod_{j=1}^{k-1} \left(1 + \psi(h)\left(\Lambda_j - \theta_j\right)\right) \tag{22}$$

also holds for all $k = 2, 3, \ldots, K$.

Proof. We prove the statements for X_k and N_k separately.

Step 1. First, we prove, by induction, that $X_k \geq 0$ with $S_k > 0$ and $I_k > 0$ for $k = 1, 2, 3, \ldots, K$.

The statement of the theorem for X_1 holds. Now, according to the induction hypothesis, $X_{k-1} \geq 0$ with $S_{k-1} > 0$, $I_{k-1} > 0$ for some $k \in [2, K]$. Thus, we obviously have $N_{k-1} > 0$ and $I_{k-1} < N_{k-1}$.

Now we express (20) in the following form:

$$\begin{aligned}
S_k =& \left[1 - \psi(h)\left(\alpha_{k-1} + \theta_{k-1} + \frac{\beta_{k-1}}{N_{k-1}}(\xi I_{k-1} + (1-\xi) I_k)\right)\right] S_{k-1} \\
&+ \psi(h)(\Lambda_{k-1} N_{k-1} + \lambda_{k-1} R_{k-1} + \nu_{k-1} B_{k-1})], \\
E_k =& \, [1 - \psi(h)(\omega_{k-1} + \theta_{k-1})] E_{k-1} + \psi(h) \frac{\beta_{k-1}}{N_{k-1}} (S_{k-1} + V_{k-1})(\xi I_{k-1} + (1-\xi) I_k), \\
I_k =& \frac{1 - \psi(h)(\xi(\gamma_{k-1} + \rho_{k-1}) + \theta_{k-1})}{1 + \psi(h)(1-\xi)(\gamma_{k-1} + \rho_{k-1})} I_{k-1} + \frac{\psi(h)\omega_{k-1}}{1 + \psi(h)(1-\xi)(\gamma_{k-1} + \rho_{k-1})} E_{k-1}, \\
R_k =& [1 - \psi(h)(\lambda_{k-1} + \theta_{k-1})] R_{k-1} + \psi(h)\gamma_{k-1}(\xi I_{k-1} + (1-\xi) I_k) + \psi(h)\sigma_{k-1} H_{k-1}, \\
V_k =& \left[1 - \psi(h)\left(\mu_{k-1} + \theta_{k-1} + \frac{\beta_{k-1}}{N_{k-1}}(\xi I_{k-1} + (1-\xi) I_k)\right)\right] V_{k-1} + \psi(h)\alpha_{k-1} S_{k-1}, \\
B_k =& [1 - \psi(h)(\nu_{k-1} + \theta_{k-1})] B_{k-1} + \psi(h)\mu_{k-1} V_{k-1}, \\
H_k =& [1 - \psi(h)(\sigma_{k-1} + \tau_{k-1} + \theta_{k-1})] H_{k-1} + \psi(h)\rho_{k-1}(\xi I_{k-1} + (1-\xi) I_k).
\end{aligned} \tag{23}$$

Applying (21), we proceed in the following manner:

1. From the I Equation (23), it follows that

$$\begin{aligned}
I_k &< \frac{2 - \psi(h)((\gamma_{k-1} + \rho_{k-1})\xi + \theta_{k-1})}{2 + \psi(h)(1-\xi)(\gamma_{k-1} + \rho_{k-1})} (I_{k-1} + E_{k-1}) \\
&\leq \frac{2 - \psi(h)((\gamma_{k-1} + \rho_{k-1})\xi + \theta_{k-1})}{2 + \psi(h)(1-\xi)(\gamma_{k-1} + \rho_{k-1})} N_{k-1} \\
&< N_{k-1}.
\end{aligned} \tag{24}$$

   According to our inductive assumption, we have $I_{k-1} > 0$, and condition (21) ensures that $2 - \psi(h)((\gamma_{k-1} + \rho_{k-1})\xi + \theta_{k-1}) > 0$. Hence, $I_k > 0$.
2. Now, we consider the S equation in (23). Since $S_{k-1} > 0$, by applying (24) and $I_{k-1} < N_{k-1}$, we obtain

$$\begin{aligned}
S_k \geq& [1 - \psi(h)(\alpha_{k-1} + \theta_{k-1} + \beta_{k-1})] S_{k-1} \\
&+ \psi(h)[\Lambda_{k-1} N_{k-1} + \lambda_{k-1} R_{k-1} + \nu_{k-1} B_{k-1}].
\end{aligned}$$

   Furthermore, condition (21) implies that $1 - \psi(h)(\alpha_{k-1} + \theta_{k-1} + \beta_{k-1}) > 0$, and we conclude that $S_k > 0$.
3. By applying (24) and $I_{k-1} < N_{k-1}$ to the E equation and V equation in (23), we obtain $E_k \geq 0$ and $V_k \geq 0$. The R equation and B equation yield $R_k \geq 0$ and $B_k \geq 0$, respectively.
4. Finally, let us consider the H equation in (23). Condition (21) ensures that the coefficient is $1 - \psi(h)(\sigma_{k-1} + \tau_{k-1} + \theta_{k-1}) > 0$. Additionally, by taking into account that $H_{k-1} \geq 0$, we obtain $H_k \geq 0$.

Therefore, the statement of the theorem for X_k holds.

Step 2. Now, we prove (22). By summing all the equations from (20), we derive the following:

$$\frac{N_k - N_{k-1}}{\psi(h)} = (\Lambda_{k-1} - \theta_{k-1})N_{k-1} - \tau_{k-1}H_{k-1},$$

$k = 2, 3, \ldots, K$.

Consequently, we find that

$$N_k = [1 + \psi(h)(\Lambda_{k-1} - \theta_{k-1})]N_{k-1} - \psi(h)\tau_{k-1}H_{k-1}. \tag{25}$$

From (25), taking into account that $\psi(h) > 0, \tau_{k-1} \geq 0$ and $H_{k-1} \geq 0$, by removing the negative term, it follows directly that

$$N_k \leq [1 + \psi(h)(\Lambda_{k-1} - \theta_{k-1})]N_{k-1}. \tag{26}$$

Since, the inequalities (26) hold for $k = 2, 3, \ldots, K$, it follows that (22)holds as well.

The proof is complete. □

Our next goal is to formulate an appropriate discrete inverse problem related to the difference scheme (20).

In accordance with this, we define the following quantities for ease of notation:

$$G_k := E_k + I_k, \quad k = 2, \ldots, K. \tag{27}$$

$$I_{\beta,k-1} := \frac{\beta_{k-1}}{N_{k-1}}(\xi I_{k-1} + (1 - \xi)I_k), \quad k = 2, \ldots, K. \tag{28}$$

$$I_{\gamma,k-1} := \gamma_{k-1}(\xi I_{k-1} + (1 - \xi)I_k), \quad k = 2, \ldots, K. \tag{29}$$

$$I_{\rho,k-1} := \rho_{k-1}(\xi I_{k-1} + (1 - \xi)I_k), \quad k = 2, \ldots, K. \tag{30}$$

$$H_{\sigma,k-1} := \sigma_{k-1}H_{k-1}, \quad k = 2, \ldots, K, \tag{31}$$

$$H_{\tau,k-1} := \tau_{k-1}H_{k-1}, \quad k = 2, \ldots, K. \tag{32}$$

By discretizing with a step size of $h = 1\,day$ and applying Equations (27)–(32), we rewrite (20) in the following form:

$$\begin{aligned}
\frac{S_k - S_{k-1}}{\psi(1)} &= -\left(\alpha_{k-1} + \theta_{k-1} + I_{\beta,k-1}\right)S_{k-1} + \Lambda_{k-1}N_{k-1} \\
&\quad + \lambda_{k-1}R_{k-1} + \nu_{k-1}B_{k-1}, \\
\frac{E_k - E_{k-1}}{\psi(1)} &= -(\omega_{k-1} + \theta_{k-1})E_{k-1} + (S_{k-1} + V_{k-1})I_{\beta,k-1}, \\
\frac{I_k - I_{k-1}}{\psi(1)} &= -I_{\gamma,k-1} - I_{\rho,k-1} - \theta_{k-1}I_{k-1} + \omega_{k-1}E_{k-1}, \\
\frac{R_k - R_{k-1}}{\psi(1)} &= -(\lambda_{k-1} + \theta_{k-1})R_{k-1} + I_{\gamma,k-1} + H_{\sigma,k-1}, \\
\frac{V_k - V_{k-1}}{\psi(1)} &= -\left(\mu_{k-1} + \theta_{k-1} + I_{\beta,k-1}\right)V_{k-1} + \alpha_{k-1}S_{k-1}, \\
\frac{B_k - B_{k-1}}{\psi(1)} &= -(\nu_{k-1} + \theta_{k-1})B_{k-1} + \mu_{k-1}V_{k-1}, \\
\frac{H_k - H_{k-1}}{\psi(1)} &= -\theta_{k-1}H_{k-1} - H_{\tau,k-1} - H_{\sigma,k-1} + I_{\rho,k-1},
\end{aligned} \tag{33}$$

Furthermore, discretizing Equation (5) with a step size of $h = 1\,day$ and again applying Equations (27)–(32) , we derive the following supplementary relationships:

$$\frac{Rtotal_k - Rtotal_{k-1}}{\psi(1)} = I_{\gamma,k-1} + H_{\sigma,k-1}, \tag{34}$$

$$\frac{Htotal_k - Htotal_{k-1}}{\psi(1)} = I_{\rho,k-1}, \tag{35}$$

$$\frac{Vtotal_k - Vtotal_{k-1}}{\psi(1)} = a_{k-1}N_{k-1}, \tag{36}$$

$$\frac{Dtotal_k - Dtotal_{k-1}}{\psi(1)} = H_{\tau,k-1}, \tag{37}$$

where $Rtotal_k = Rtotal(t_k)$, $Htotal_k = Htotal(t_k)$, $Vtotal_k = Vtotal(t_k)$ and $Dtotal_k = Dtotal(t_k)$.

Next, following [28,29], we introduce the notations for the officially reported data:

$$\begin{aligned} m_k &:= (A_k,\, H_k,\, Rtotal_k,\, Dtotal_k,\, Vtotal_k,\, Htotal_k) \\ &= (A(t_k),\, H(t_k),\, Rtotal(t_k),\, Dtotal(t_k),\, Vtotal(t_k), Htotal(t_k)), \end{aligned}$$

and for the unknown values

$$g_k := (S_k,\, E_k,\, I_k,\, R_k,\, V_k,\, B_k),$$

where $k = 1, 2, \ldots, K$.

Then, we categorize the parameters $(\{p_k\}_{k=1}^{K})$ into two separate groups:

- A group consisting of parameters whose values are naturally assumed to be known:

$$q_k := (\Lambda_k,\, \theta_k,\, \omega_k,\, \mu_k,\, \nu_k,\, \lambda_k,\, \varphi_k),$$

where we add the daily values (φ_k) of vaccine effectiveness;

- A group consisting of parameters whose values we need to find:

$$r_k := (\alpha_k,\, \beta_k,\, \gamma_k,\, \varrho_k,\, \sigma_k,\, \tau_k).$$

To analyze the dynamics of COVID-19, we now formulate an inverse problem. To do this, we determine the parameters of system (1) using official reported data.

Inverse Problem $(P_{inv}(\xi, \psi))$: Let $\xi \in [0, 1]$ be fixed and the values of g_1, $\{q_k\}_{k=1}^{K-1}$ and $\{m_k\}_{k=1}^{K}$be given. Then, find the quantities of$\big(\{g_k(\xi, \psi)\}_{k=2}^{K}, \{r_{k-1}(\xi, \psi)\}_{k=2}^{K}\big)$ such that relations (33)–(37) hold.

It is important to note again that inverse problems are typically ill-posed.

To solve inverse problem $P_{inv}(\xi, \psi)$, first of all, we sum up the second and third equations in the discretized scheme (33). Then, applying (27) and notations (27)–(32), we obtain the following relations:

$$\begin{aligned} S_k &= \Big[1 - \psi(1)\Big(\alpha_{k-1} + \theta_{k-1} + I_{\beta,k-1}\Big)\Big] S_{k-1} \\ &\quad + \psi(1)(\Lambda_{k-1}N_{k-1} + \lambda_{k-1}R_{k-1} + \nu_{k-1}B_{k-1}), \\ I_k &= [1 - \psi(1)(\theta_{k-1} + \omega_{k-1})]I_{k-1} + \psi(1)\Big(\omega_{k-1}G_{k-1} - I_{\gamma,k-1} - I_{\rho,k-1}\Big), \\ G_k &= [1 - \psi(1)\theta_{k-1}]G_{k-1} + \psi(1)\Big((S_{k-1} + V_{k-1})I_{\beta,k-1} - I_{\gamma,k-1} - I_{\rho,k-1}\Big), \\ R_k &= [1 - \psi(1)(\lambda_{k-1} + \theta_{k-1})]R_{k-1} + \psi(1)(I_{\gamma,k-1} + H_{\sigma,k-1}), \\ V_k &= \Big[1 - \psi(1)(\mu_{k-1} + \theta_{k-1} + I_{\beta,k-1})\Big] V_{k-1} + \psi(1)\alpha_{k-1}S_{k-1}, \\ B_k &= [1 - \psi(1)(\nu_{k-1} + \theta_{k-1})]B_{k-1} + \psi(1)\mu_{k-1}V_{k-1}, \\ H_k &= [1 - \psi(1)\theta_{k-1}]H_{k-1} + \psi(1)\Big(I_{\rho,k-1} - H_{\tau,k-1} - H_{\sigma,k-1}\Big). \end{aligned} \tag{38}$$

Based on these findings, we can now outline the following procedure.

Unique Solving Algorithm for the Inverse Problem $P_{inv}(\xi, \psi)$**:** Assume that the non-negative data values of $A_k, G_k, H_k, Dtotal_k, Rtotal_k, Htotal_k$, and $Vtotal_k$ are given for $k = 1, 2, \ldots, K$, along with the initial non-negative values of $S_1, G_1, I_1, R_1, V_1, B_1$, and H_1 and their sum (N_1), where $S_1 > 0$ and $G_1 \geq I_1 > 0$. Using this information, $E_1 = G_1 - I_1$ is also determined, and we compute the sequences of $\{g_k(\xi, \psi)\}_{k=2}^{K}$ and $\{r_{k-1}(\xi, \psi)\}_{k=2}^{K}$ according to the steps described below.

1. According to (27), non-hospitalized active cases are expressed as

$$G_k = A_k - H_k, \quad k = 1, 2, \ldots, K.$$

2. Using (32), we obtain

$$H_{\tau,k-1} = \frac{Dtotal_k - Dtotal_{k-1}}{\psi(1)}, \quad k = 2, \ldots, K.$$

3. According to (35), we find that

$$I_{\rho,k-1} = \frac{Htotal_k - Htotal_{k-1}}{\psi(1)}, \quad k = 2, \ldots, K.$$

4. From the H_k equation in (38), we obtain

$$H_{\sigma,k-1} = \frac{H_{k-1} - H_k}{\psi(1)} - H_{\tau,k-1} - \theta_{k-1} H_{k-1} + I_{\rho,k-1}, \quad k = 2, \ldots, K.$$

5. According to (34), we find that

$$I_{\gamma,k-1} = \frac{Rtotal_k - Rtotal_{k-1}}{\psi(1)} - H_{\sigma,k-1}, \quad k = 2, \ldots, K.$$

6. Let us now assume that the values of S_{k-1}, I_{k-1}, R_{k-1}, V_{k-1}, G_{k-1}, and therefore N_{k-1} for some $k \in [1, K-1]$ are calculated and $N_{k-1} > 0$, $S_{k-1} + V_{k-1} > 0$. Then,

   - Taking into account that $\alpha_{k-1} = \varphi_{k-1} a_{k-1}$ and according to (36), for $k = 2, \ldots, K$, we obtain the vaccination parameter:

$$\alpha_{k-1} = \varphi_{k-1} \frac{Vtotal, k - Vtotal_{k-1}}{\psi(1) N_{k-1}}.$$

   - Using the G_k equation from (38), we calculate

$$I_{\beta,k-1} = \frac{1}{S_{k-1} + V_{k-1}} \left[\frac{G_k - G_{k-1}}{\psi(1)} + \theta_{k-1} G_{k-1} + I_{\gamma,k-1} + I_{\rho,k-1} \right].$$

   - By means of the I_k equation, R_k equation, V_k equation, B_k equation, and S_k equation in (38), we compute I_k, R_k, V_k, B_k, and S_k sequentially.
   - Using (27), we find

$$E_k = G_k - I_k.$$

   - Finally, the value of N_k

$$N_k = S_k + E_k + I_k + R_k + V_k + B_k + H_k$$

is also obtained. In this way, the values of S_k, E_k, I_k, R_k, V_k, B_k, H_k, N_k, $k = 1, 2, \ldots, K$ are calculated sequentially.

7. Now, according to Equations (28)–(32), the parameters are computed as follows for $k = 2, \ldots, K$:

$$\begin{aligned} \beta_{k-1}(\xi) &= N_{k-1}\frac{I_{\beta,k-1}}{\xi I_{k-1} + (1-\xi)I_k}, \\ \gamma_{k-1}(\xi) &= \frac{I_{\gamma,k-1}}{\xi I_{k-1} + (1-\xi)I_k}, \\ \rho_{k-1}(\xi) &= \frac{I_{\rho,k-1}}{\xi I_{k-1} + (1-\xi)I_k}, \\ \sigma_{k-1} &= \frac{H_{\sigma,k-1}}{H_{k-1}}, \\ \tau_{k-1} &= \frac{H_{\tau,k-1}}{H_{k-1}}, \end{aligned} \tag{39}$$

8. Should any step yield a biologically unreasonable value, the algorithm must terminate.

Finally, taking into account Remark 4, we consider the following family of simple functions:

$$\psi_c(h) = h + c\,h^2, \tag{40}$$

where a constant is $c > -1/h$. Furthermore, in Section 6 we apply the Algorithm for Solving the Inverse Problem ($P_{inv}(\xi, \psi)$) using different functions ($\psi_c(h)$), i.e., different c values. Since $\psi_c(1) = 1 + c$, the computed function values and parameter values obtained by this algorithm depend on the choice of c.

Remark 5. *The backward Euler scheme is a widely used method for finite-difference approximation of time-derivative terms in complex evolution models. Its primary advantage is that it is unconditionally stable. However, it offers only first-order accuracy. It is also well known that higher-order schemes generally require sufficiently small time steps to maintain stability. In this study, this approach is not applicable due to the fact that we fixed the time step to 1 day. Under this constraint, the choice of $\psi(h) = h + ch^2$ becomes natural. Enhanced accuracy is then achieved by optimizing the parameter to $c > -1$ within the family of finite-difference schemes generated by the perturbation ($\psi(1) = 1 + c$). In the next section, we show that this approach yields a substantial improvement in accuracy while preserving the non-negativity of the numerical solution.*

6. Solving the Discrete Inverse Problems for the SEIRS-VBH Model and Validation

To validate the SEIRS-VBH model, we use officially reported data for COVID-19 in Bulgaria [47–50] for the time frame of 7 June 2020–12 March 2023. The reported cases for 7 June 2020 are used as the initial data, and we consider an additional 1008 days (144 weeks) for the simulation, i.e., $t_k = k$, $k = 1, 2, \ldots, K$, $K = 1009$. We assume that the official information provided each morning refers to the data from the previous day; for example, the 1019 reported active cases on 8 June 2020 are considered as the A_1 value corresponding to 7 June 2020.

We use data on Bulgaria's population, as well as annual birth and mortality rates from [51], together with data on COVID-19 deaths reported in [47], to calculate N_1 and the following daily values for birth and natural mortality rates: $\Lambda = (0.2459 \times 10^{-4}, 0.2493 \times 10^{-4}, 0.2411 \times 10^{-4}, 0.2477 \times 10^{-4}$ and $\theta = (0.3815 \times 10^{-4}, 0.5296 \times 10^{-4}, 0.4737 \times 10^{-4}, 0.4277 \times 10^{-4})$ for the days of 2020, 2021, 2022, and 2023, respectively. Then, in accordance with [30], we assume that the reinfection rates of recovered and vacci-

nated individuals are equal to $\lambda(t) = \nu(t) := 1/180$ and the antibody rate is $\mu(t) := 1/14$. Finally, for the latency rate , we use $\omega(t) := (1/7^1, 1/6^2, 1/5^3, 1/4^4)$, and for the vaccine effectiveness rates, we use $\varphi(t) := (0.85^2, 0.70^3, 0.45^4)$ for the ^{1} Wuhan variant; ^{2} Alpha, Beta, and Gamma variants; ^{3} Delta variant; and ^{4} Omicron variant of SARS-CoV-2.

It should be noted that the *Vtotal* group includes individuals who completed the full recommended course of vaccination, as well as those who received the booster dose. The latter are considered newly vaccinated individuals who have lost their vaccine-acquired immunity.

To solve the discrete inverse problem ($P_{inv}(\xi, \psi)$), then to validate the model, we introduce the grid expressed as

$$\Pi := \{(\xi_i, c_j) = ((i-1)/200, -0.25 + (j-1)/200),\ i = 1, 2, 3, \ldots, 201;\ j = 1, 2, 3, \ldots, 101\}.$$

Now, we describe the results from the conducted numerical experiments.

First of all, for each node (ξ_i, c_j) of the grid (Π), we perform the following steps:

Step 1 (Parameter identification). Using the Unique Solving Algorithm from Section 5, we solve the discrete inverse problem ($P_{inv}(\xi_i, \psi_j)$) with the $\psi_j(h) = h + c_j h^2$ function and $h = 1$ day. As a result, we obtain the following non-negative parameter values:

$$r_{k-1}(\xi_i, c_j) := (\alpha_{k-1}(\xi_i, c_j), \beta_{k-1}(\xi_i, c_j), \gamma_{k-1}(\xi_i, c_j), \rho_{k-1}(\xi_i, c_j), \sigma_{k-1}(c_j), \tau_{k-1}(c_j)),$$

$k = 2, 3, \ldots, K$ and

$$g_k(\xi_i, c_j) := (S_k(\xi_i, c_j),\ E_k(\xi_i, c_j),\ I_k(\xi_i, c_j),\ R_k(\xi_i, c_j),\ V_k(\xi_i, c_j),\ B_k(\xi_i, c_j)),$$

$k = 1, 2, \ldots, K$. Graphics of the parameter values obtained for particular values of ξ and c are provided in Appendix A.2.

Step 2 (Extended direct problem solving). We use the parameter values obtained in Step 1 and numerically solve the extended direct problem (1), (2) and (5), (6) (with $t_0 = t_1$) with initial conditions of $S(t_1) = S_1$, $E(t_1) = E_1$, $I(t_1) = I_1$, $R(t_1) = R_1$, $V(t_1) = V_1$, $B(t_1) = B_1$, $H(t_1) = H_1$ and $Rtotal(t_1) = Rtotal_1$, $Vtotal(t_1) = Vtotal_1$, $Htotal(t_1) = Htotal_1$, $Dtotal(t_1) = Dtotal_1$. More precisely, we solve the extended Cauchy problem for the second day (t_2) (using the initial data from t_1). Then for each next day (t_k), the problem is solved again with constant parameters of $\beta_{k-1}(\xi_i, c_j), \gamma_{k-1}(\xi_i, c_j), \rho_{k-1}(\xi_i, c_j), \sigma_{k-1}(c_j), \tau_{k-1}(c_j)$, where the computed values of the $(S, E, I, R, V, B, H, Rtotal, Vtotal, Htotal, Dtotal)$ functions at the end of the previous day (t_{k-1}) serve as the initial data for the current day. This means that only the initial data for the first day are prescribed, while those for the following days are computed. This computation is performed using the ode45 solver in Matlab, which implements the Runge–Kutta 4th/5th-order method with a step size of 0.01 on each interval ($[t_{k-1}, t_k]$), and as a result, we obtain the numerical solution:

$$X_{\xi_i, c_j}(t) = (S_{\xi_i, c_j}(t), E_{\xi_i, c_j}(t), I_{\xi_i, c_j}(t), R_{\xi_i, c_j}(t), V_{\xi_i, c_j}(t), B_{\xi_i, c_j}(t), H_{\xi_i, c_j}(t))$$

and

$$Y_{\xi_i, c_j}(t) = (Rtotal_{\xi_i, c_j}(t), Vtotal_{\xi_i, c_j}(t), Htotal_{\xi_i, c_j}(t_n), Dtotal_{\xi_i, c_j}(t))$$

for $t = t_1 + n/100$, $n = 0, 1, \ldots, 100(K-1)$.

Graphics of the components of $X_{\xi_i, c_j}(t)$ for special values of ξ and c, as defined in Step 4, are presented in Appendix A.3. Let us mention that all values obtained by this procedure are biologically reasonable.

Step 3 (l_2 and l_∞ relative errors calculation). Let us introduce the notation for the official reported numbers of active cases, hospitalized individuals, total recoveries, total vaccinations, total hospitalizations, and total deaths:

$$\begin{aligned}
A_{reported} &:= (A_1, A_2, \ldots, A_K),\\
H_{reported} &:= (H_1, H_2, \ldots, H_K),\\
Rtotal_{reported} &:= (Rtotal_1, Rtotal_2, \ldots, Rtotal_K),\\
Vtotal_{reported} &:= (Vtotal_1, Vtotal_2, \ldots, Vtotal_K),\\
Htotal_{reported} &:= (Htotal_1, Htotal_2, \ldots, Htotal_K),\\
Dtotal_{reported} &:= (Dtotal_1, Dtotal_2, \ldots, Dtotal_K).
\end{aligned}$$

For the corresponding computed values at the end of each day, we use the following notations:

$$\begin{aligned}
A_{computed}(\xi_i, c_j) &:= (A_{\xi_i,c_j}(t_1), A_{\xi_i,c_j}(t_2), \ldots, A_{\xi_i,c_j}(t_K)),\\
H_{computed}(\xi_i, c_j) &:= (H_{\xi_i,c_j}(t_1), H_{\xi_i,c_j}(t_2), \ldots, H_{\xi_i,c_j}(t_K)),\\
Rtotal_{computed}(\xi_i, c_j) &:= (Rtotal_{\xi_i,c_j}(t_1), Rtotal_{\xi_i,c_j}(t_2), \ldots, Rtotal_{\xi_i,c_j}(t_K)),\\
Vtotal_{computed}(\xi_i, c_j) &:= (Vtotal_{\xi_i,c_j}(t_1), Vtotal_{\xi_i,c_j}(t_2), \ldots, Vtotal_{\xi_i,c_j}(t_K)),\\
Htotal_{computed}(\xi_i, c_j) &:= (Htotal_{\xi_i,c_j}(t_1), Htotal_{\xi_i,c_j}(t_2), \ldots, Htotal_{\xi_i,c_j}(t_K)),\\
Dtotal_{computed}(\xi_i, c_j) &:= (Dtotal_{\xi_i,c_j}(t_1), Dtotal_{\xi_i,c_j}(t_2), \ldots, Dtotal_{\xi_i,c_j}(t_K)),
\end{aligned}$$

where the calculated active cases are

$$A_{\xi_i,c_j}(t_k) := E_{\xi_i,c_j}(t_k) + I_{\xi_i,c_j}(t_k) + H_{\xi_i,c_j}(t_k).$$

Then, we compute the relative errors as

$$\begin{aligned}
Error(l_2, \xi_i, c_j) :=& \frac{\|A_{reported} - A_{computed}(\xi_i, c_j)\|_2}{\|A_{reported}\|_2} + \frac{\|H_{reported} - H_{computed}(\xi_i, c_j)\|_2}{\|H_{reported}\|_2}\\
&+ \frac{\|Rtotal_{reported} - Rtotal_{computed}(\xi_i, c_j)\|_2}{\|Rtotal_{reported}\|_2}\\
&+ \frac{\|Vtotal_{reported} - Vtotal_{computed}(\xi_i, c_j)\|_2}{\|Vtotal_{reported}\|_2}\\
&+ \frac{\|Htotal_{reported} - Htotal_{computed}(\xi_i, c_j)\|_2}{\|Htotal_{reported}\|_2}\\
&+ \frac{\|Dtotal_{reported} - Dtotal_{computed}(\xi_i, c_j)\|_2}{\|Dtotal_{reported}\|_2}
\end{aligned}$$

and

$$\begin{aligned}
Error(l_\infty, \xi_i, c_j) :=& \frac{\|A_{reported} - A_{computed}(\xi_i, c_j)\|_\infty}{\|A_{reported}\|_\infty} + \frac{\|H_{reported} - H_{computed}(\xi_i, c_j)\|_\infty}{\|H_{reported}\|_\infty}\\
&+ \frac{\|Rtotal_{reported} - Rtotal_{computed}(\xi_i, c_j)\|_\infty}{\|Rtotal_{reported}\|_\infty}\\
&+ \frac{\|Vtotal_{reported} - Vtotal_{computed}(\xi_i, c_j)\|_\infty}{\|Vtotal_{reported}\|_\infty}\\
&+ \frac{\|Htotal_{reported} - Htotal_{computed}(\xi_i, c_j)\|_\infty}{\|Htotal_{reported}\|_\infty}\\
&+ \frac{\|Dtotal_{reported} - Dtotal_{computed}(\xi_i, c_j)\|_\infty}{\|Dtotal_{reported}\|_\infty}.
\end{aligned}$$

The results are presented in Figures 2 and 3. We observe that the proposed modified discrete difference schemes improve both the standard explicit ($\xi = 1$) and semi-implicit ($0 \leq \xi < 1$) schemes. The relative errors ($Error(l_2, \xi, c)$ and $Error(l_\infty, \xi, c)$) for the modified explicit (forward) Euler scheme ($\xi = 1$) are lowest for small positive values of c. In contrast, for the modified semi-implicit schemes ($\xi = 0$), both errors are smallest for small negative values of c. On the other hand, for each fixed c value, the obtained results show that the explicit Euler scheme produces the largest relative errors, but weighted convex linear combinations of backward and forward Euler schemes can provide higher accuracy while, at the same time, maintaining stability.

Step 4 (Model validation). To validate the SEIRS-VBH model, we minimize both relative errors computed in Step 3 on the grid (Π):

$$\min_{(\xi,c)\in\Pi} Error(l_2, \xi, c) = Error(l_2, 0.41, -0.005) = 0.0251$$

and

$$\min_{(\xi,c)\in\Pi} Error(l_\infty, \xi, c) = Error(l_\infty, 0.41, -0.005) = 0.0273.$$

This result shows that both relative errors achieved their minimum on the grid (Π) at one and the same node, i.e.,

$$(\xi^*, c^*) := (0.41, -0.005).$$

Hence, among all considered discrete inverse problems ($P_{inv}(\xi_i, \psi_j)$) the solution expressed as $\{r_{k-1}(\xi^*, c^*)\}_{k=2}^K$, $\{g_k(\xi^*, c^*)\}_{k=1}^K$ of $P_{inv}(\xi^*, \psi^*)$, where $\psi^* := h + c^* h^2$ with $h = 1$, provides the best approximation of the reported data.

The documentation of the relative errors ($Error(l_2, \xi^*, c)$ and $Error(l_\infty, \xi^*, c)$) in Table 2 shows that relative errors provided by the modified difference schemes with $c = c^*$ are about four times lower than the relative error provided by the standard difference scheme ($c = 0$).

Table 2. Documentation of the relative errors ($Error(l_2, \xi, c)$ and $Error(l_\infty, \xi, c)$) for $\xi = \xi^*$ and $c = -0.03 \div 0.02$.

c	-0.03	-0.025	-0.02	-0.015	-0.01	-0.005	0	0.005	0.01	0.015	0.02
l_2	0.4498	0.3631	0.2749	0.1855	0.0963	0.0251	0.1009	0.1967	0.2951	0.3956	0.4980
l_∞	0.4637	0.3765	0.2878	0.1975	0.1055	0.0273	0.0960	0.1882	0.2849	0.3848	0.4866

By minimizing the investigated relative errors on the grid (Π), we identify the best of the considered approximations to the officially reported data. In this way, the SEIRS-VBH model is validated.

The curves of reported ($A_{reported}$) and computed ($A_{computed}(\xi^*, c^*)$) active cases are compared in Figure 4. A comparison of remaining reported and computed data is shown in Appendix A.1 as follows: *Rtotal* in Figure A1, *Vtotal* in Figure A2, *Htotal* in Figure A3, and *Dtotal* in Figure A4. In all these figures, we observe very good agreement between the reported data and the data computed with the SEIRS-VBH model.

Remark 6. *In Figure 4, the reported and model plots appear to coincide mainly because of the length of the time period and large changes in values. However, in reality, this is not the case, as clearly shown in Figure 5, where the values are visualized only for the period of 6–13 February 2022, which, in the real situation, corresponds to the highest peak of active cases on 10 February 2022. The situation is similar with the plots in the figures presented in Appendix A.1, where, at first glance, the plots appear identical. They are consistent with the low values of the relative errors computed in*

our analysis. One can easily verify this by executing the corresponding scripts from the GitHub repository (see Data Availability Statement) and inspecting the plots in greater detail by zooming in.

The obtained parameter values of $\{r_{k-1}(\xi^*, c^*)\}_{k=2}^{K}$ are presented in Appendix A.2. The behavior of the parameters over time, as well as the 7-day moving averages, are shown as follows: $\alpha(\xi^*, c^*)$ in Figure A5, $\beta(\xi^*, c^*)$ in Figure A6, $\gamma(\xi^*, c^*)$ in Figure A7, $\varrho(\xi^*, c^*)$ in Figure A8, $\sigma(c^*)$ in Figure A9, and $\tau(c^*)$ in Figure A10.

The solution (X_{ξ^*,c^*}) of the SEIRS-VBH model (direct problem (1), (2)) is presented graphically in Appendix A.3. Graphics of the components are shown as follows: infectious (I_{ξ^*,c^*}) and vaccinated susceptible (V_{ξ^*,c^*}) in Figure A11, exposed (E_{ξ^*,c^*}) and hospitalized (H_{ξ^*,c^*}) in Figure A11, disease-acquired (R_{ξ^*,c^*}) and vaccine-acquired immunity (B_{ξ^*,c^*}) in Figure A13, and susceptible (S_{ξ^*,c^*}) and total population size $(N_{\xi^*,c^*} := S_{\xi^*,c^*} + E_{\xi^*,c^*} + I_{\xi^*,c^*} + R_{\xi^*,c^*} + V_{\xi^*,c^*} + B_{\xi^*,c^*} + H_{\xi^*,c^*})$ in Figure A14.

In order to demonstrate and quantify the advantage of the proposed SEIRS-VBH model and the performance of its validation methodology, we compare our results with a reference simulation based on a standard SEIR model. The inverse problem for the SEIR model was formulated and analyzed in our previous work [52], where an explicit Euler scheme was employed. Following the latter approach here, we identify the parameters of the SEIR model and subsequently solve the corresponding direct problem. For the SEIR model, the comparison between the computed and reported data for active cases and recovered individuals yields the following errors: an l_2 error of 0.3544, and an l_∞ error of 0.3612. These errors are more than ten times larger than the relative errors ($Error(l_2, \xi^*, c^*)$ and $Error(l_\infty, \xi^*, c^*)$) for the SEIRS-VBH model obtained in the present paper. This reduction in error highlights the clear advantage of the SEIRS-VBH model, which provides a substantially better fit to the reported data.

7. SEIRSVBH Simulator: Description and Usage

The SEIRSVBH Simulator is a MATLAB-based tool developed by the authors of this paper, referred to hereinafter as "the simulator". The simulator consists of two distinct components:

- A script-based computational module intended for large-scale data processing, model calibration, and reproduction of the results presented in this research;
- A graphical user interface (GUI), which enables intuitive interaction, parameter manipulation, and visual exploration of simulation results (see Figure 6).
  All results presented in this paper were obtained exclusively through the script-based component of the simulator.

The simulator operates using officially reported data on the COVID-19 pandemic, caused by the SARS-CoV-2 virus, for Bulgaria for the period of 7 June 2020–12 March 2023, enabling data-driven analysis of the pandemic's evolution across this full time frame.

The simulator further integrates MATLAB's parallel processing framework as a core computational feature, allowing for concurrent evaluation of multiple (ξ, c) parameter combinations. This design substantially reduces computation time and enhances the scalability and performance of error quantification and parameter inference procedures, enabling efficient large-scale simulations.

The SEIRSVBH Simulator adds scientific value by integrating all stages of the computational workflow—error analysis, parameter evaluation, and model validation—within a consistent graphical environment. It serves to facilitate transparent and reproducible analysis of the COVID-19 disease dynamics using officially reported COVID-19 data for Bulgaria, providing researchers with an accessible platform for conducting, visualizing, and validating epidemiological simulations.

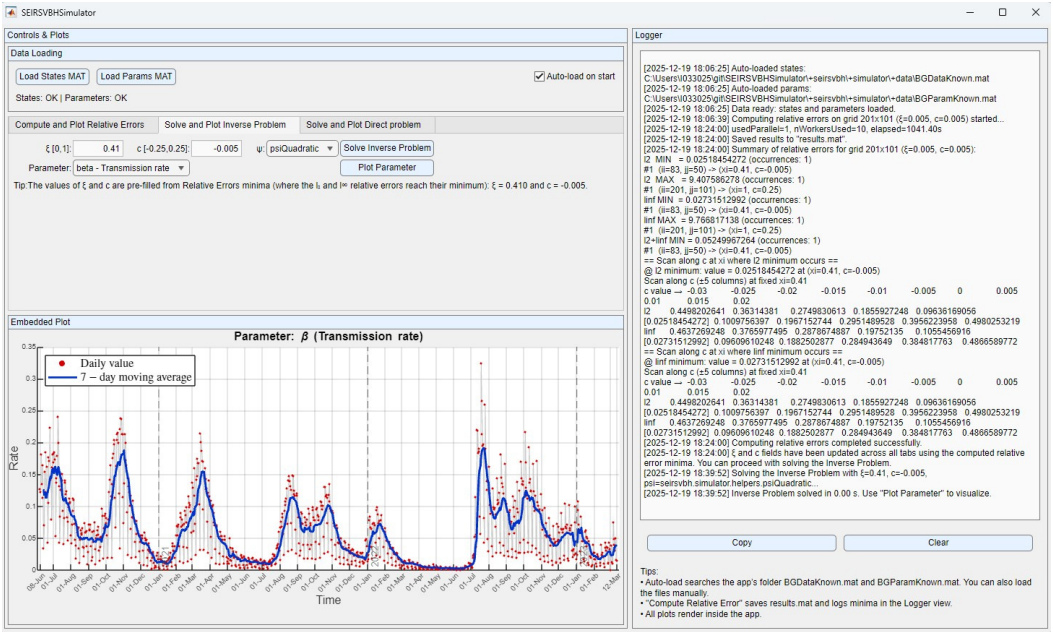


Figure 6. Graphical interface of the SEIRSVBH Simulator.

8. Discussion

Here, we note that the SEIRS-VBH model does not explicitly incorporate the values of the transmission or recovery rates of non-hospitalized and hospitalized individuals, as these parameters depend on factors such as social distancing measures, treatment methods, and the intrinsic characteristics of the virus. The precise functional dependence among these factors remains unknown. To overcome this limitation, we address this issue by formulating and solving an appropriate inverse problem to estimate the daily parameter values (see Appendix A.2) that mathematically represent the complex behavior of the official reported data. This is why the parameter values are sensitive to changes in the data. For example, the rapid decline in the reported number of active cases (see Figure 4), which results from the sharp increase in the reported number of recovered individuals (Figure A1) during June 2022 leads to an elevated recovery rate among non-hospitalized individuals (Figure A7). However, this does not significantly affect the recovery rate of hospitalized individuals (Figure A9), as the number of hospitalized patients at that time (Figure A12) was much lower than the number of individuals reported to have recovered. These events are followed by increases in the transmission rate (Figure A6) and hospitalization rate (Figure A8) caused by the emergence of the omicron variant in Bulgaria. This example of parameter behavior demonstrates that the model works effectively with real-world data, even in the presence of abrupt changes.

It is also worth noting that, with the exception of hospitalized individuals, there are no officially reported data for the components of the SEIRS-VBH model solution. The proposed methodology for solving an extended inverse problem allows the size of important groups to be calculated (see Appendix A.3) as exposed, infectious, and susceptible (vaccinated and non-vaccinated) individuals, as well as people with vaccine-acquired immunity and disease-acquired immunity.

All these results can be very useful in the accurate calculation of key epidemiological characteristics, such as basic and effective reproduction values and the herd immunity threshold.

9. Conclusions

Our study provides a methodology based on real-world data for computing the time behavior of important epidemiological indicators, such as the transmission rate, the recovery rates of hospitalized and non-hospitalized individuals, the number of people with vaccine-acquired immunity, and the number of individuals with disease-acquired immunity. It is shown that the available official reported COVID-19 data is sufficient for calculating these indicators. For this purpose, a novel deterministic model with biologically reasonable properties is proposed. An appropriate inverse problem was formulated and investigated through a time-discrete approach. A modified semi-implicit difference scheme was used, and the error at a step of 1 day was estimated for a time period of 1009 days. The numerical experiments demonstrate that the utilized non-standard weighted difference schemes significantly improve the accuracy of the calculations. The model validation shows very good agreement between computed and officially reported data.

Author Contributions: Conceptualization, T.H.; methodology, S.M., N.P. and T.H.; investigation, S.M., N.P., T.H. and V.K.; software, T.H. and V.K.; validation, T.H. and V.K.; visualization, T.H. and V.K.; writing—original draft preparation, N.P., T.H. and V.K.; writing—review and editing, S.M. All authors have read and agreed to the published version of the manuscript.

Funding: The work of S. Margenov and N. Popivanov was partially supported by the Centre of Excellence in Informatics and ICT under Grant No. BG16RFPR002-1.014-0018-C01, financed by the Research, Innovation, and Digitalization for Smart Transformation Programme 2021–2027 and co-financed by the European Union. The work of N. Popivanov and V. Koleva was partially supported by Sofia University under Grant 80-10-74/2025.

Data Availability Statement: The data presented in this study are openly available on GitHub at https://github.com/venetakoleva/SEIRSVBHSimulator (accessed on 14 December 2025).

Acknowledgments: The authors thank the anonymous referees for making several helpful suggestions.

Conflicts of Interest: The authors declare no conflicts of interest.

Abbreviations

The following abbreviations are used in this manuscript:

WHO	World Health Organization
SARS-CoV-2	Severe acute respiratory syndrome coronavirus 2
COVID-19	Coronavirus disease 2019
ODEs	Ordinary differential equations
SIR	Susceptible–Infectious–Recovered
SEIRS	Susceptible–Exposed–Infectious–Recovered–Susceptible
SEIRS-VBH	Susceptible–Exposed–Infectious–Recovered–Susceptible–Vaccinated Susceptible–Vaccinated Immune–Hospitalized

Appendix A. Visualizations of the Results from the Numerical Experiments

This section contains graphical representations of the time behavior of the parameters, as well as that of the solution of the SEIRS-VBH model. A comparison of the reported data with those calculated using the model is also presented.

Appendix A.1. Results from Validation

Results from comparison of the reported and computed data with $\xi = \xi^* = 0.41$, $c = c^* = -0.005$ in Step 4, Section 6 are reported as follows.

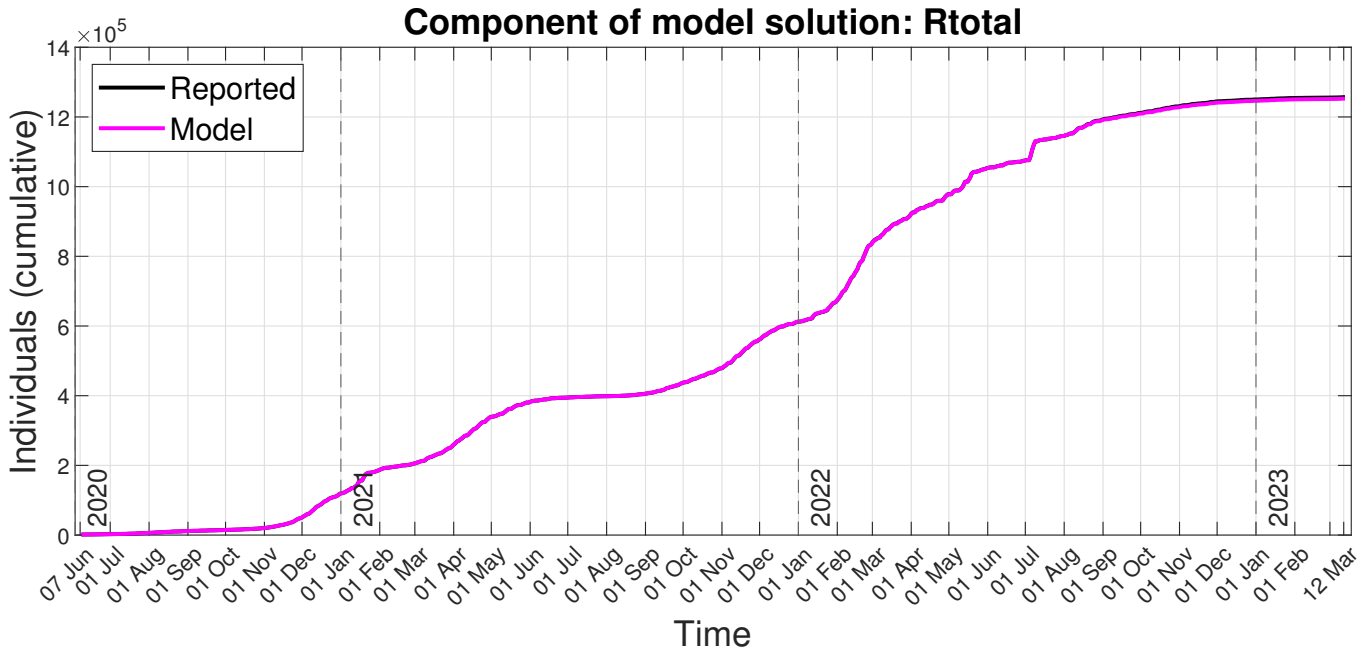


Figure A1. Reported cases ($Rtotal_{reported}$) and model curve ($Rtotal_{computed}(\xi^*, c^*)$) of cumulative number of recovered individuals.

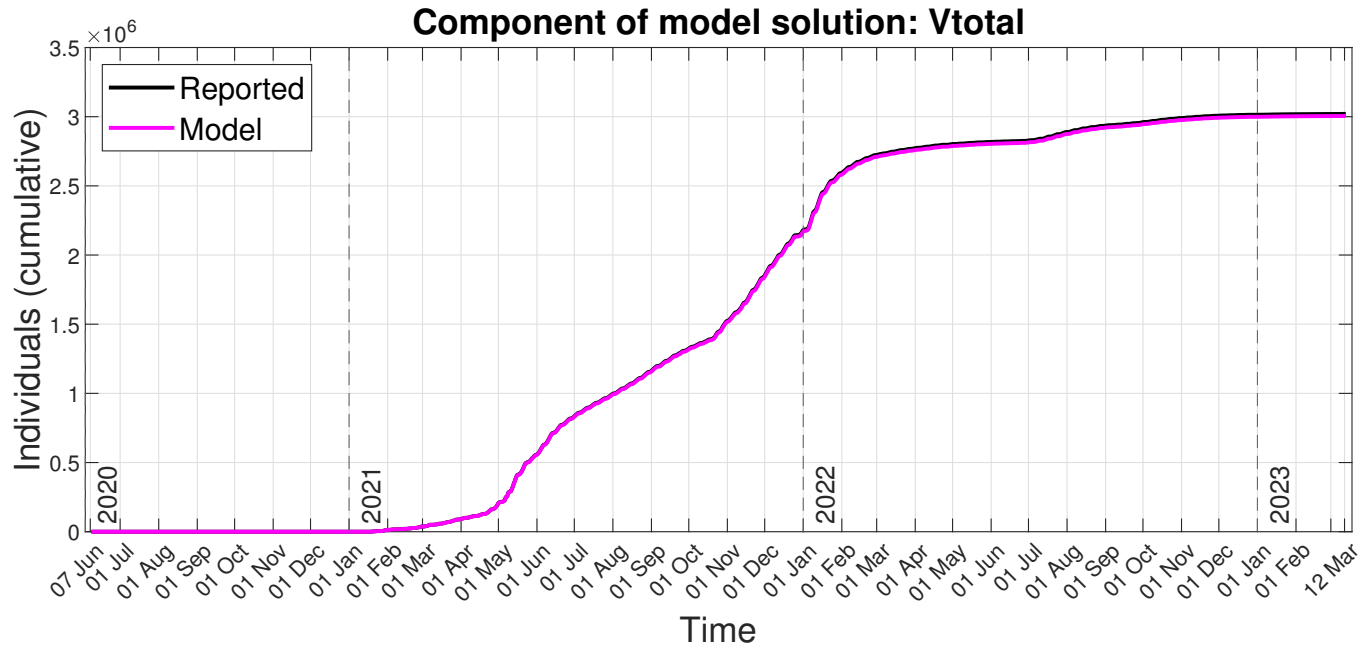


Figure A2. Reported cases ($Vtotal_{reported}$) and model curve ($Vtotal_{computed}(\xi^*, c^*)$) of cumulative number of vaccinated individuals.

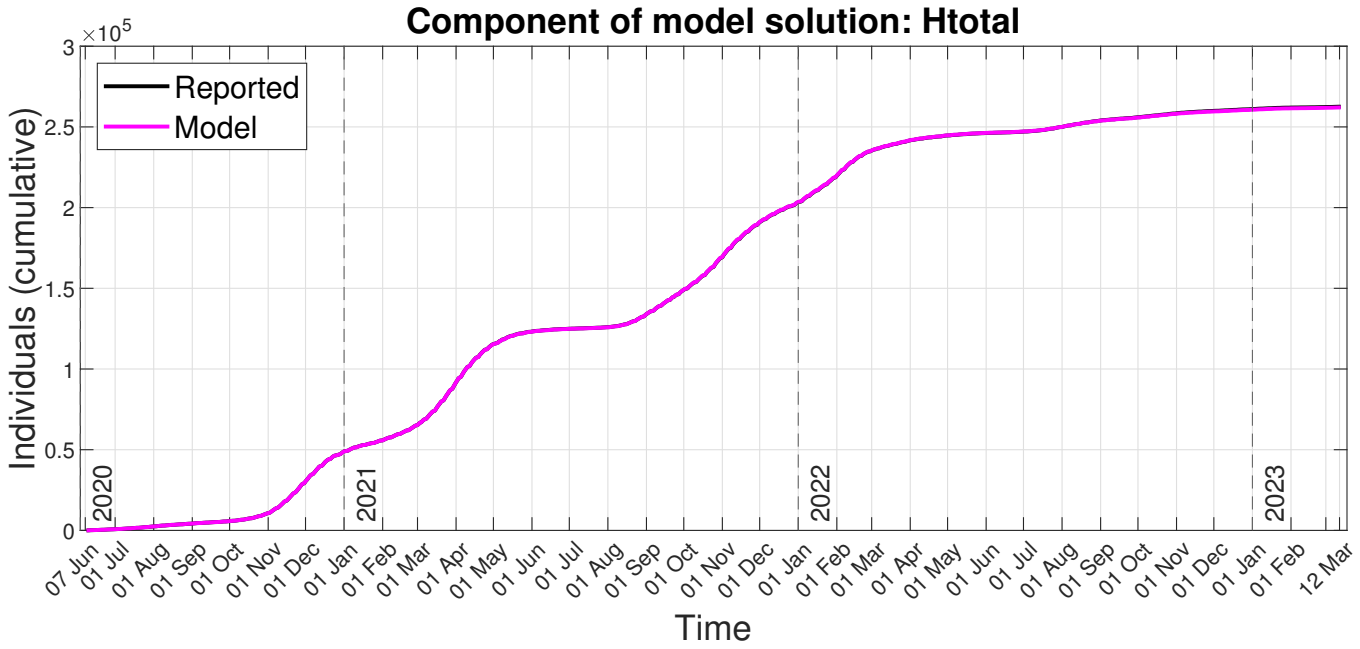


Figure A3. Reported cases ($Htotal_{reported}$) and model curve ($Htotal_{computed}(\xi^*, c^*)$) of cumulative number of hospitalized individuals.

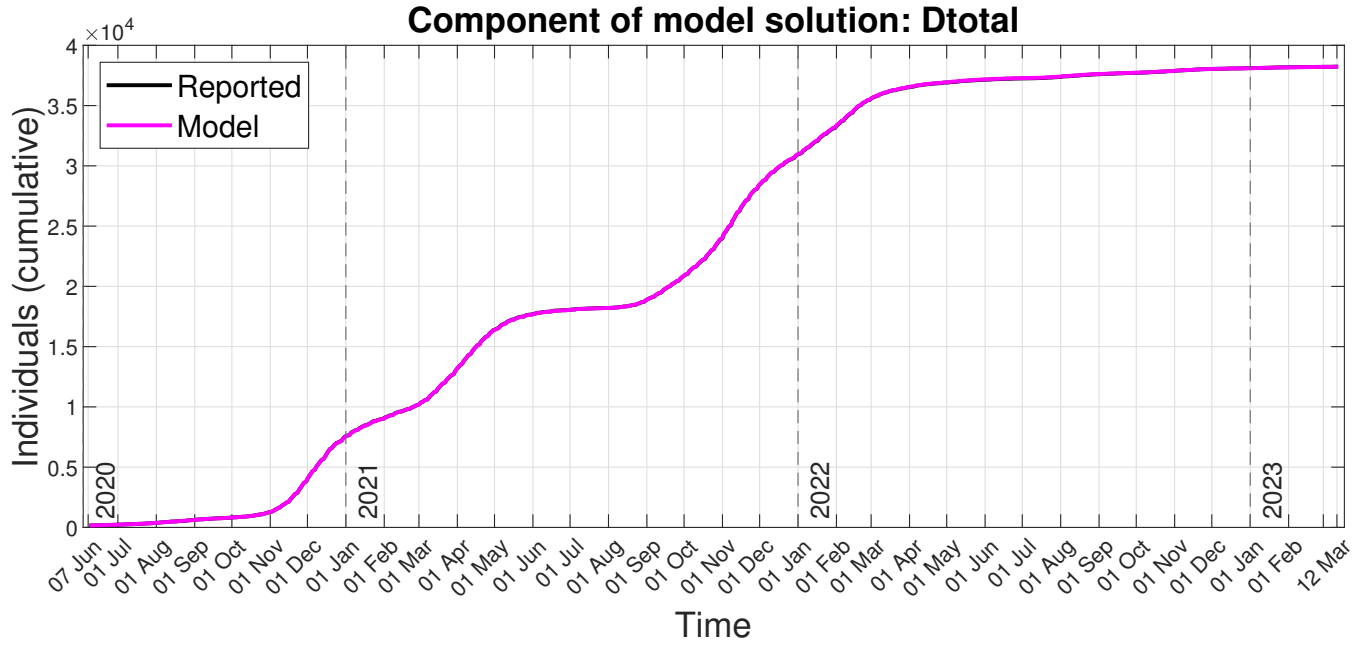


Figure A4. Reported cases ($Dtotal_{reported}$) and model curve ($Dtotal_{computed}(\xi^*, c^*)$) of cumulative number of COVID-19 deaths.

Appendix A.2. Computed Model' Parameters

Results from the computation of parameters with $\xi = \xi^* = 0.41, c = c^* = -0.005$ in Step 1, Section 6 are reported as follows.

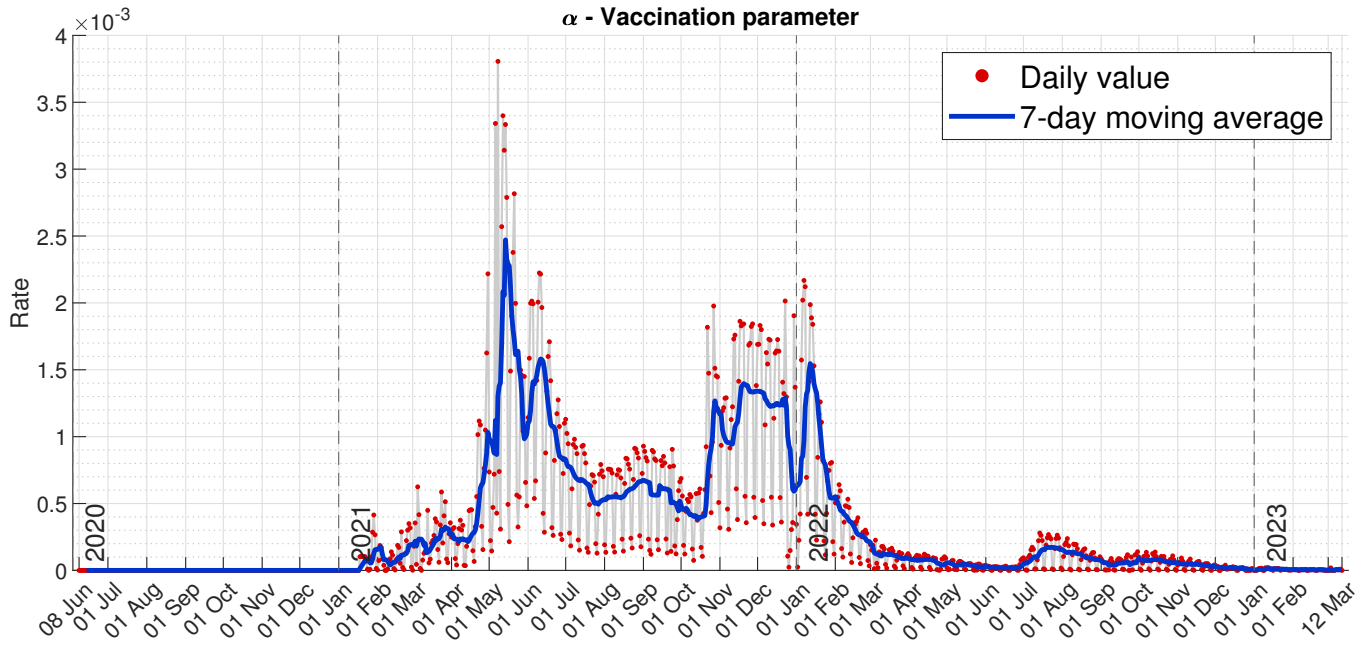


Figure A5. Vaccination parameter ($\alpha(\xi^*, c^*)$).

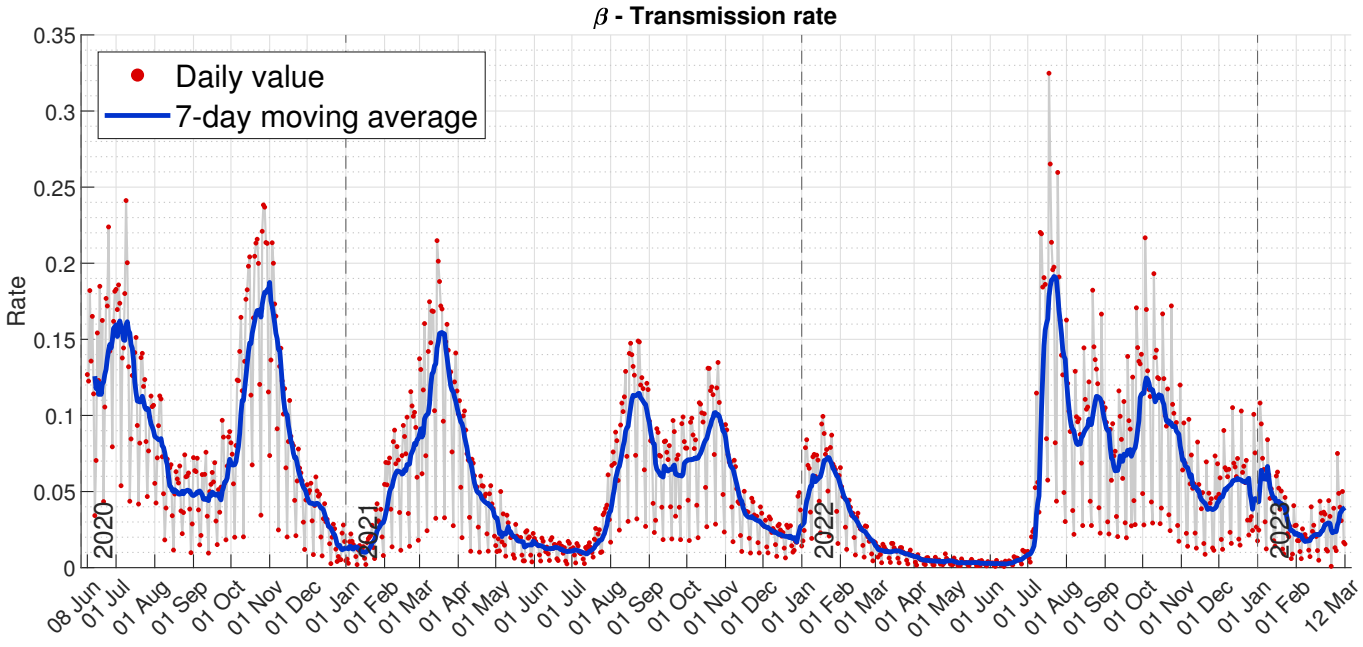


Figure A6. Transmission rate ($\beta(\xi^*, c^*)$).

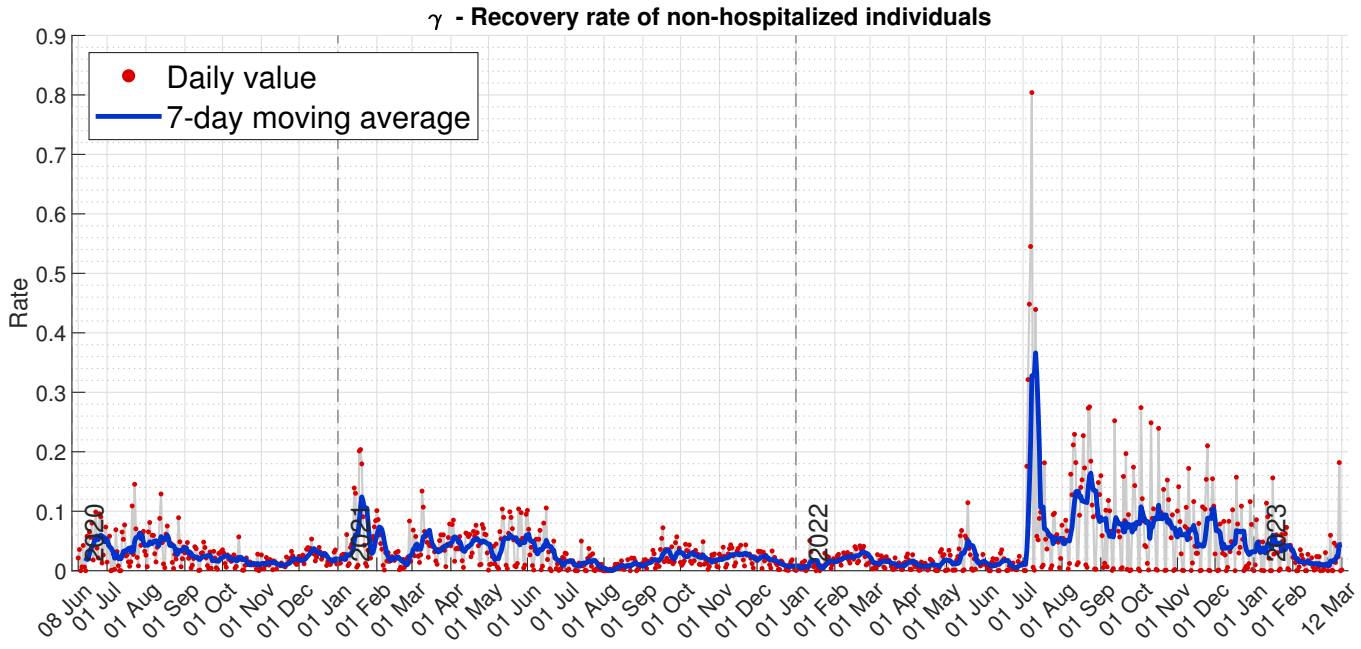


Figure A7. Recovery rate of non-hospitalized individuals ($\gamma(\xi^*, c^*)$).

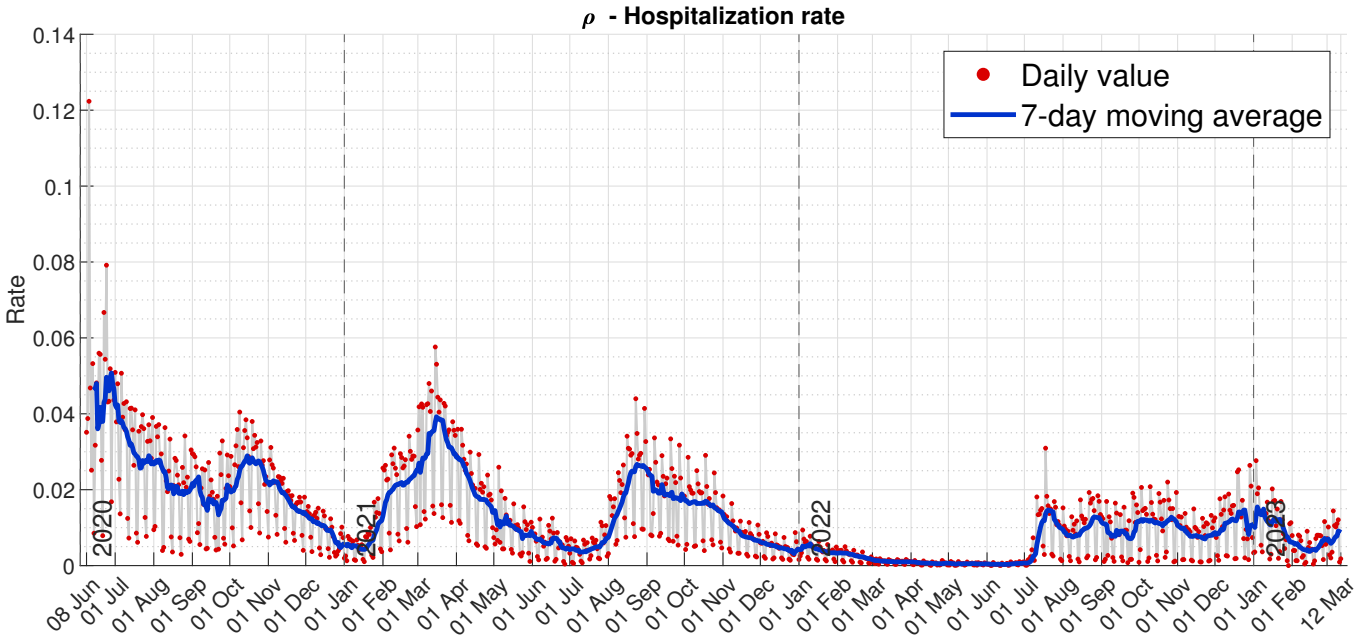


Figure A8. Hospitalization rate ($\varrho(\xi^*, c^*)$).

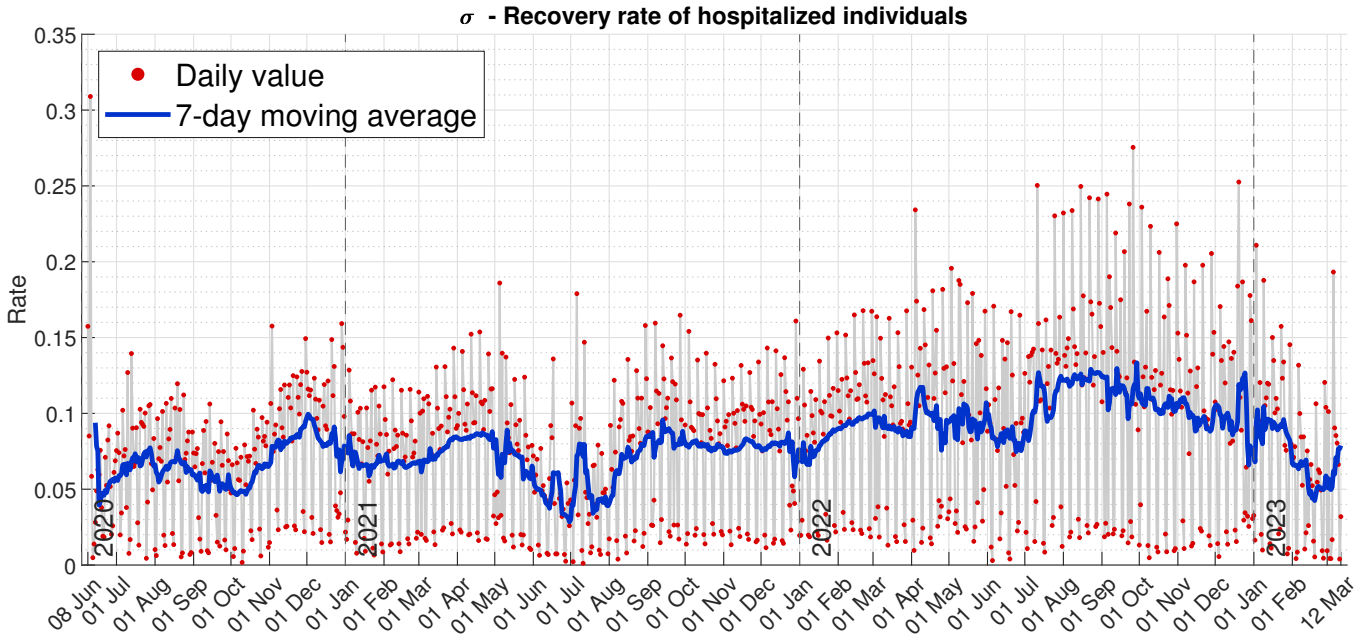


Figure A9. Recovery rate of hospitalized individuals ($\sigma(c^*)$).

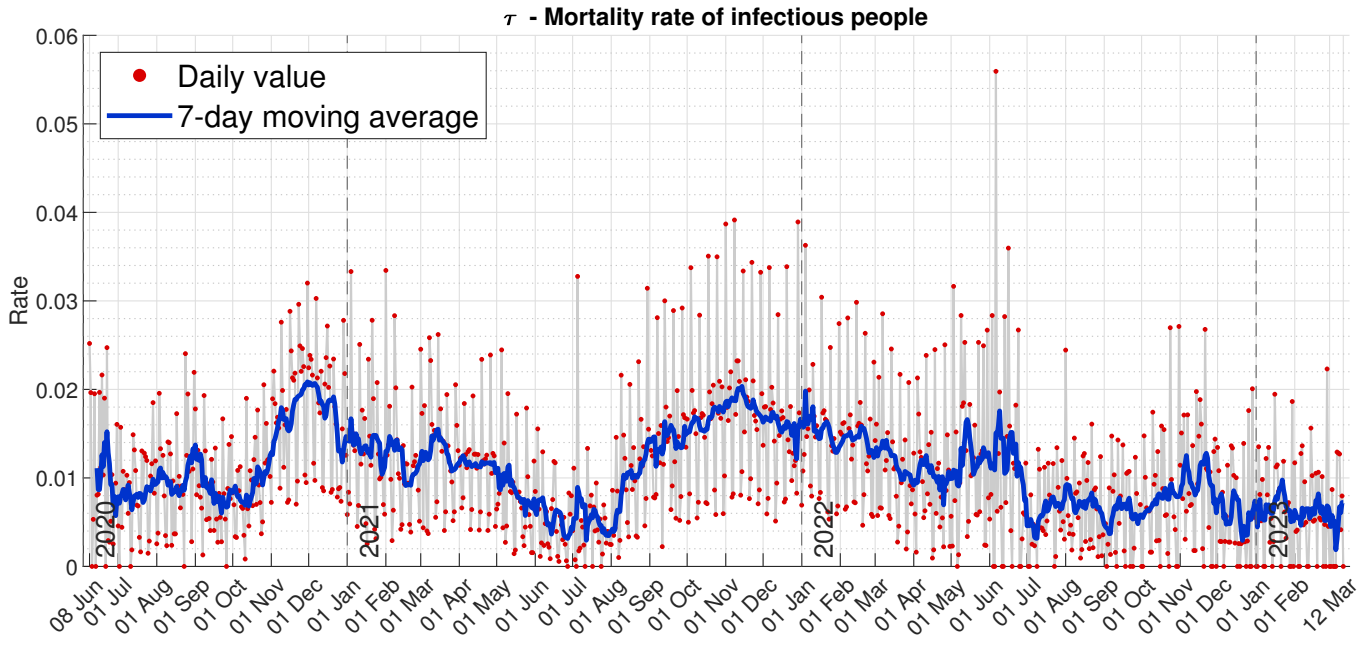


Figure A10. Mortality rate of infectious people ($\tau(c^*)$).

Appendix A.3. The Model Solution

Results from the computation of the model solution with $\xi = \xi^* = 0.41, c = c^* = -0.005$ in Step 2, Section 6 are reported as follows.

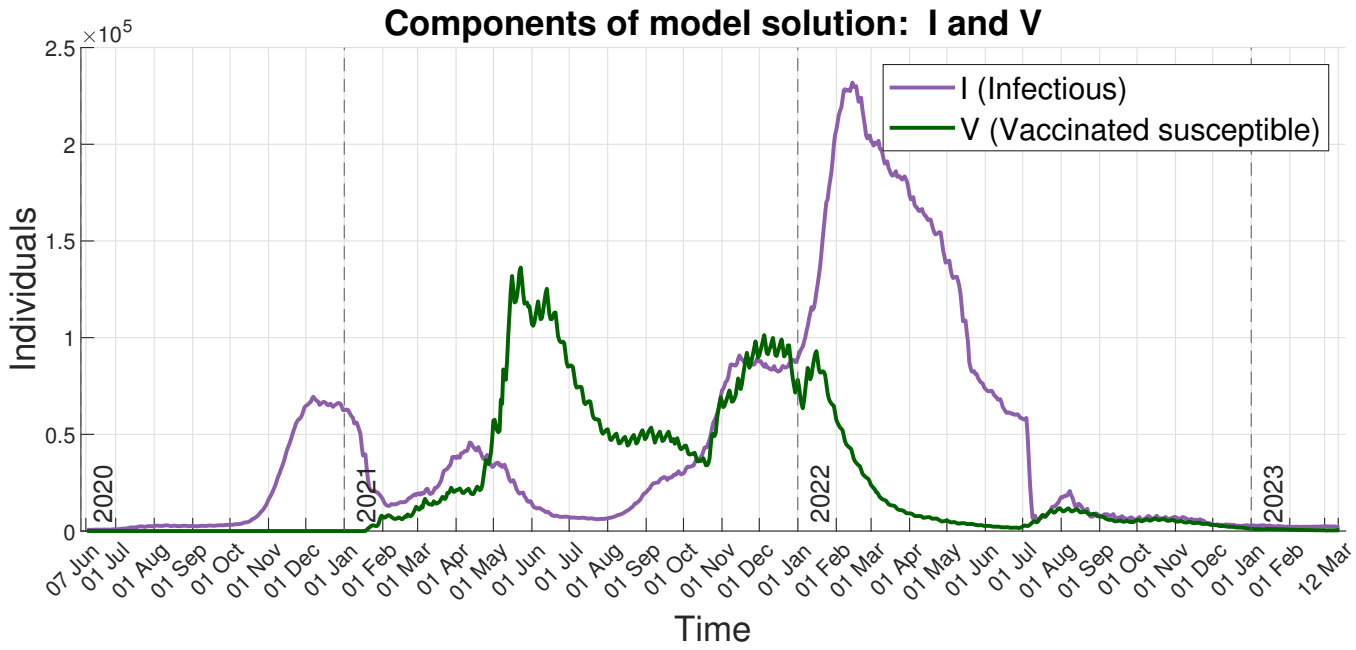


Figure A11. Components of the direct problem solution: infectious (I_{ξ^*,c^*}) and vaccinated susceptible (V_{ξ^*,c^*}) individuals.

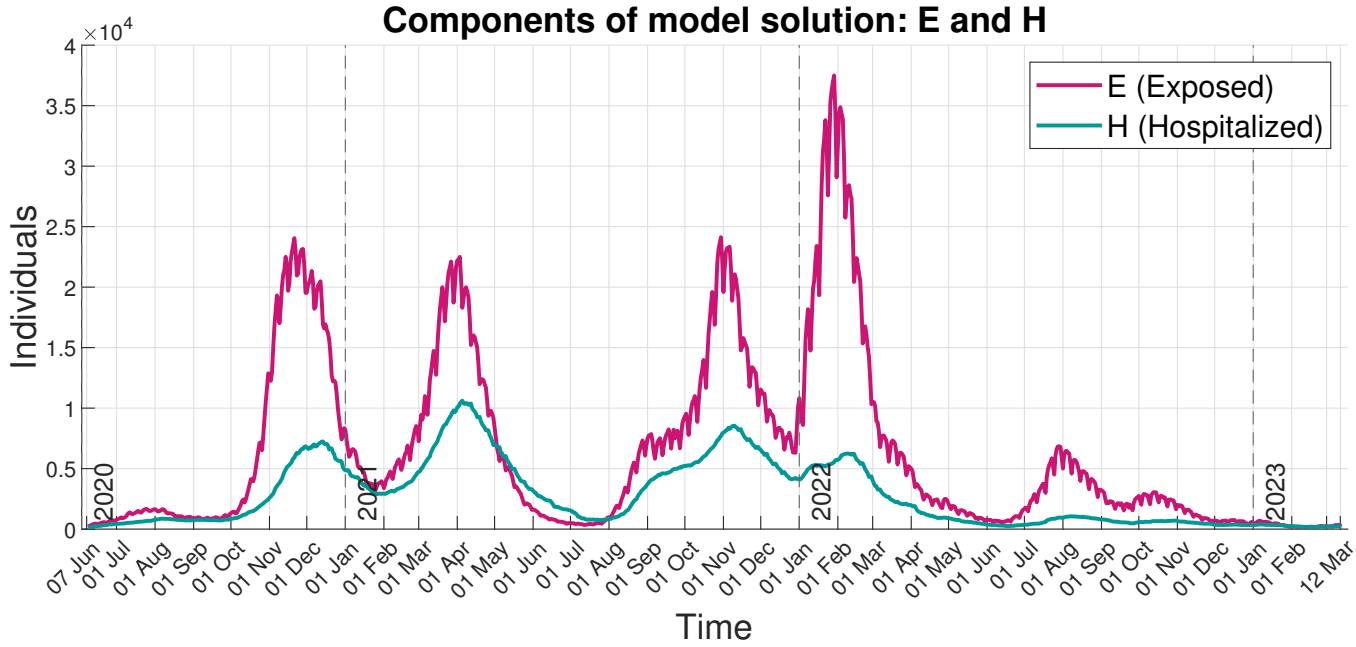


Figure A12. Components of the direct problem solution: exposed (E_{ξ^*,c^*}) and hospitalized (H_{ξ^*,c^*}) individuals.

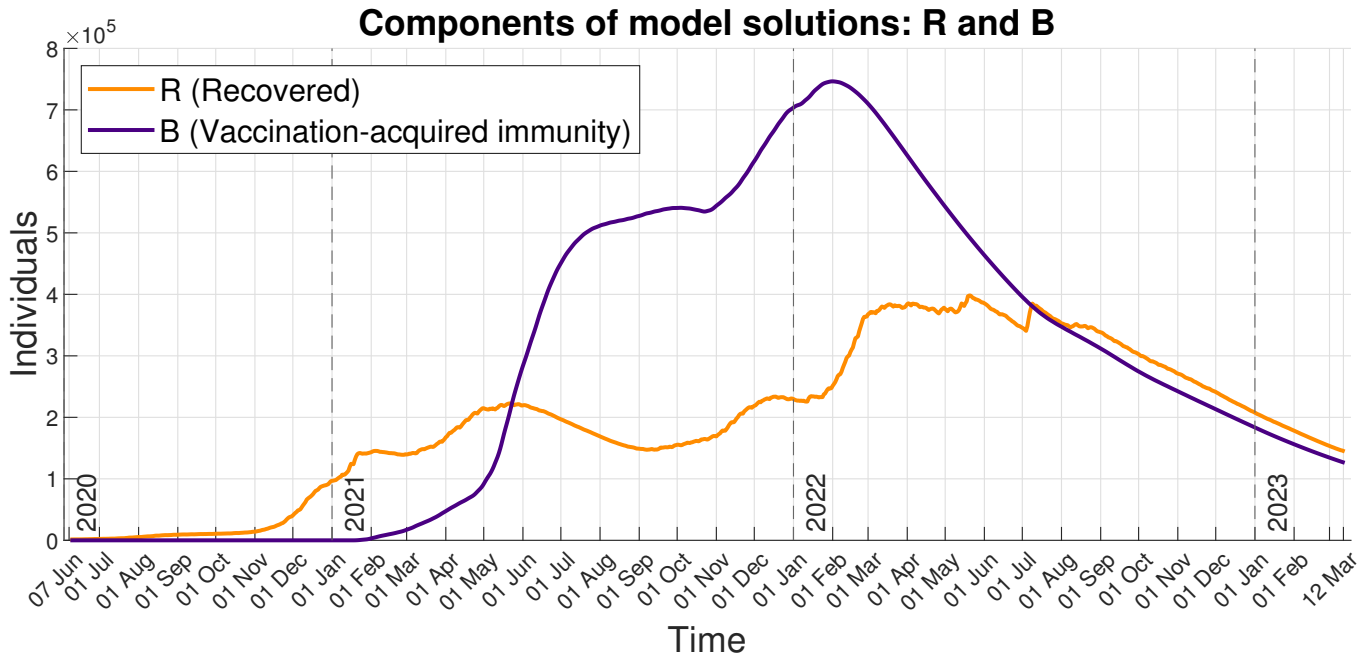


Figure A13. Components of the direct problem solution: recovered individuals (S_{ξ^*,c^*}) and those with vaccine-acquired immunity (B_{ξ^*,c^*}).

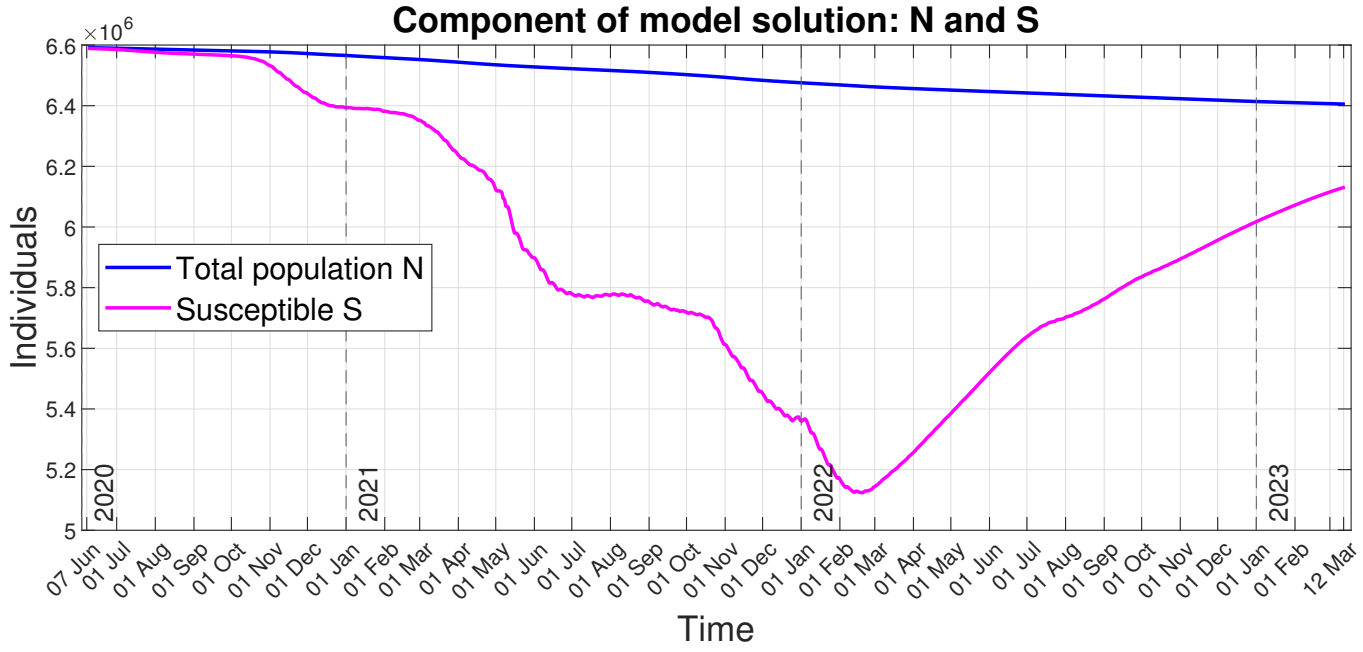


Figure A14. Components of the direct problem solution: susceptible individuals (S_{ξ^*,c^*}) and total population size (N_{ξ^*,c^*}).

References

1. Li, Y.; Wang, L.-W.; Peng, Z.-H.; Shen, H.-B. Basic reproduction number and predicted trends of coronavirus disease 2019 epidemic in the mainland of China. *Infect. Dis. Poverty* **2020**, *9*, 94. [CrossRef]
2. World Health Organization. WHO COVID-19 Dashboard. Available online: https://data.who.int/dashboards/covid19 (accessed on 14 October 2025).
3. Martcheva, M. *An Introduction to Mathematical Epidemiology*; Texts in Applied Mathematics; Springer: New York, NY, USA, 2015; Volume 61, p. 453. [CrossRef]
4. Kadri, A.; Boudaoui, A.; Ullah, S.; Asiri, M.; Saqib, A.B.; Riaz, M.B. A comparative study of deterministic and stochastic computational modeling approaches for analyzing and optimizing COVID-19 control. *Sci. Rep.* **2025**, *15*, 11710. [CrossRef]

5. Flaig, J.; Houy, N. Epidemic control using stochastic and deterministic transmission models: Performance comparison with and without parameter uncertainties. *medRxiv* **2022**. [CrossRef]
6. Velásquez, R.; Lara, J. Forecast and evaluation of COVID-19 spreading in USA with reduced-space Gaussian process regression. *Chaos Solitons Frac.* **2020**, *136*, 109924. [CrossRef]
7. Carcione, J.; Santos, J.; Bagaini, C.; Ba, J. A Simulation of a COVID-19 Epidemic Based on a Deterministic SEIR Model. *Front. Public Health* **2020**, *8*, 230. [CrossRef]
8. Aronna, M.S.; Guglielmi, R.; Mosche, L.M. A model for COVID-19 with isolation, quarantine and testing as control measures. *Epidemics* **2021**, *34*, 100437. [CrossRef]
9. Taghizadeh, E.; Mohammad-Djafari, A. SEIR Modeling, Simulation, Parameter Estimation, and Their Application for COVID-19 Epidemic. *Phys. Sci. Forum* **2022**, *5*, 18. [CrossRef]
10. Kabanikhin, S.I.; Krivorotko, O.I. Mathematical Modeling of the Wuhan COVID-2019 Epidemic and Inverse Problems. *Comput. Math. Math. Phys.* **2020**, *60*, 1889–1899. [CrossRef]
11. Miao, H.; Xia, X.; Perelson, A.S.; Wu, H. On Identifiability of Nonlinear ODE Models and Applications in Viral Dynamics. *SIAM Rev. Soc. Ind. Appl. Math.* **2011**, *53*, 3–39. [CrossRef]
12. Engl, H.W.; Hanke, M.; Neubauer, A. *Regularization of Inverse Problems*; Mathematics and Its Applications; Springer: Dordrecht, The Netherlands, 2000; Volume 375, p. 322. https://link.springer.com/book/9780792341574.
13. Kabanikhin, S.I.; Krivorotko, O.I.; Neverov, A.V. Differential Epidemic Models and Scenarios of Restrictive Measures. *Comput. Math. Math. Phys.* **2025**, *65*, 1300–1313. [CrossRef]
14. Leonov, A.S.; Nagornov, O.V.; Tyu. S.A. Inverse problem for coefficients of equations describing propagation of COVID-19 epidemic. *J. Phys. Conf. Ser.* **2021**, *2036*, 012028. [CrossRef]
15. Marinov, T.; Marinova, R. Dynamics of COVID-19 using inverse problem for coefficient identification in SIR epidemic models. *Chaos Soliton Fract. X* **2020**, *5*, 100041. [CrossRef]
16. Marinov, T.T.; Marinova, R.S. Inverse problem for adaptive SIR model: Application to COVID-19 in Latin America. *Infect. Dis. Model.* **2022**, *7*, 134–148. [CrossRef]
17. Stevens, M.; Sunseri, A.; Alexanderian, A. Hyper-differential sensitivity analysis for inverse problems governed by ODEs with application to COVID-19 modeling. *Math. Biosci.* **2022**, *351*, 108887. [CrossRef]
18. Kermack, W.; McKendrick, A. A Contribution to the Mathematical Theory of Pandemics. *Proc. R. Soc. Lond. Ser. A* **1927**, *115*, 700–721.
19. Papageorgiou, V.E.; Vasiliadis, G.; Tsaklidis, G. Analyzing the Asymptotic Behavior of an Extended SEIR Model with Vaccination for COVID-19. *Mathematics* **2024**, *12*, 55. [CrossRef]
20. Jdid, T.; Benbrahim, M.; Kabbaj, M.N.; Naji, M. A vaccination-based COVID-19 model: Analysis and prediction using Hamiltonian Monte Carlo. *Heliyon* **2024**, *10*, 19. [CrossRef]
21. Alqahtani, R.T.; Yusuf, A. Development and analysis of a SEIR model for COVID-19 epidemic with vaccination and nonsingular kernel. *Fractals* **2022**, *30*, 2240040. [CrossRef]
22. Alsaud, H.; Kulachi, M.O.; Ahmad, A.; Inc, M.; Taimoor, M. Investigation of SEIR model with vaccinated effects using sustainable fractional approach for low immune individuals. *AIMS Math.* **2024**, *9*, 10208–10234. [CrossRef]
23. Müller, G.; Ferreira, L.; Mesias Campos, F.; Borges, M.; Berg de Almeida, G.; Poloni, S.; Simon, L.; Bagattini, B.; Quarti, M.; Felizola Diniz Filho, J.; et al. Modeling the impact of child vaccination (5–11 y) on overall COVID-19 related hospitalizations and mortality in a context of omicron variant predominance and different vaccination coverage paces in Brazil. *Lancet Reg.-Health-Am.* **2023**, *17*, 100396. [CrossRef]
24. Delli Compagni, R.; Cheng, Z.; Russo, S.; Van Boeckel, T.P. A hybrid Neural Network-SEIR model for forecasting intensive care occupancy in Switzerland during COVID-19 epidemics. *PLoS ONE* **2022**, *17*, e0263789. [CrossRef]
25. Li, C-Z.; Lü, X.; Gong, J.-J.; Lei, Y. Extended SEIR model of COVID-19 spread focusing on compartmental flow in England. *Nonlinear Dyn.* **2025**, *113*, 971–988. [CrossRef]
26. Kiselev, I.N.; Akberdin, I.R.; Kolpakov, F.A. Delay-differential SEIR modeling for improved modelling of infection dynamics. *Sci. Rep.* **2023**, *13*, 13439. [CrossRef]
27. Castaceda, A.; Ramirez-Torres, E.; Valdés-García, L.; Morandeira-Padryn, H.; Yanez, D.; Montijano, J.; Bergues, L. Modified SEIR epidemic model including asymptomatic and hospitalized cases with correct demographic evolution. *Appl. Math. Comput.* **2023**, *456*, 128122. [CrossRef]
28. Margenov, S.; Popivanov, N.; Ugrinova, I.; Hristov, T. Mathematical Modeling and Short-Term Forecasting of the COVID-19 Epidemic in Bulgaria: SEIRS Model with Vaccination. *Mathematics* **2022**, *10*, 2570. [CrossRef]
29. Margenov, S.; Popivanov, N.; Ugrinova, I.; Hristov, T. Differential and Time-Discrete SEIRS Models with Vaccination: Local Stability, Validation and Sensitivity Analysis Using Bulgarian COVID-19 Data. *Mathematics* **2023**, *11*, 2238. [CrossRef]
30. Margenov, S.; Popivanov, N.; Hristov, T.; Koleva, V. Computing the COVID-19 Basic and Effective Reproduction Numbers Using Actual Data: SEIRS Model with Vaccination and Hospitalization. *Mathematics* **2024**, *12*, 3998. [CrossRef]

31. Khan, A.H. *Modeling the Spread of COVID-19 Pandemic in Morocco. Challenges in Modeling of an Outbreak's Prediction, Forecasting and Decision Making for Policy Makers*; Infosys Science Foundation Series in Mathematical Sciences; Springer: Singapore, 2021; pp. 377–408. [CrossRef]
32. Chan, Y.T. The macroeconomic impacts of the COVID-19 pandemic: A SIR-DSGE model approach. *China Econ. Rev.* **2022**, *71*, 101725. [CrossRef]
33. Pangestu, D.S.; Anggriani, N.; Yaacob, N.M. Quantifying the Health-Economy Trade-Offs: Mathematical Model of COVID-19 Pandemic Dynamics. *Computation* **2024**, *12*, 139. [CrossRef]
34. Schuh, L.; Markov, P.V.; Veliov, V.M.; Stilianakis, N.I. A mathematical model for the within-host (re)infection dynamics of SARS-CoV-2. *Math. Biosci.* **2024**, *371*, 109178. [CrossRef]
35. Shi, Y.; Zhu, X.; Zhu, X.; Cheng, B.; Zhong, Y. Kalman Filter-Based Epidemiological Model for Post-COVID-19 Era Surveillance and Prediction. *Sensors* **2025**, *25*, 2507. [CrossRef]
36. Garg, T.; Rakshit, M.; Manivel, M.; Shyamsunder. Modeling of Hepatitis B Virus Transmission With Vaccination, Treatment, and Memory Effects, *Adv. Theory Simul.* **2025**, *7*, e01358. [CrossRef]
37. Rezapour, S.; Mohammadi, H.; Samei, M.E. SEIR epidemic model for COVID-19 transmission by Caputo derivative of fractional order. *Adv. Differ. Equ.* **2020**, *490*. [CrossRef]
38. Nabi, K.H.; Abboubakar, H.; Kumar, P. Forecasting of COVID-19 pandemic: From integer derivatives to fractional derivatives. *Chaos Solitons Fractals* **2020**, *141*, 110283. [CrossRef]
39. Momani, S.; Batiha, I.M.; Bendib, I.; Al-Nana, A.; Ouannas, A. Dalah, M. On finite-time stability of some COVID-19 models using fractional discrete calculus. *Comput. Methods Programs Biomed. Update* **2025**, *7*, 100188. [CrossRef]
40. Mehdizadeh Khalsaraei, M.; Shokri, A.; Ramos, H.; Yao, S.-W.; Molayi, M. Efficient Numerical Solutions to a SIR Epidemic Model. *Mathematics* **2022**, *10*, 3299. [CrossRef]
41. Shagdar, E.-A.; Balt, B. Extending Nonstandard Finite Difference Scheme for the SEIR Epidemic Model. *J. Inst. Math. Digit. Technol.* **2022**, *4*, 16–24. [CrossRef]
42. Liu, M.; Cao, J.; Liang, J.; Chen, M. *Epidemic-Logistics Modeling: A New Perspective on Operations Research*, 1st ed.; Springer: Singapore, 2020; p. 287.
43. Hartman, P. *Ordinary Differential Equations*, 2nd ed.; Society for Industrial and Applied Mathematics: Philadelphia, PA, USA, 2002; p. 624.
44. Pontryagin, L.S. *Ordinary Differential Equations*; Pergamon Press: London, UK; Paris, France, 1962; p. 298.
45. Kirsch, A. *An Introduction to the Mathematical Theory of Inverse Problems*; Springer: Cham, Switzerland, 2021; p. 400. [CrossRef]
46. Krivorotko, O.I.; Kabanikhin, S.I. On mathematical models of COVID-19 pandemic. *Sib. Elektron. Mat. Izv.* **2023**, *20*, 1211–1268.
47. Worldometers, The Coronavirus Tracker. Available online: https://www.worldometers.info/coronavirus/ (accessed on 27 August 2025).
48. Ministry of Health of the Republic of Bulgaria: The Open Data Portal of the Republic of Bulgaria. Available online: https://testdata.egov.bg (accessed on 27 August 2025).
49. MAPEX: Map of COVID 19 in Bulgaria. Available online: https://covid.tobel.bg/Home/About (accessed on 27 August 2025).
50. The Official Bulgarian Unified Information Portal. Available online: https://coronavirus.bg/ (accessed on 15 March 2023).
51. World Bank Open Data. Available online: https://data.worldbank.org/indicator?tab=all (accessed on 19 September 2025).
52. Margenov, S.; Popivanov, N.; Ugrinova, I.; Harizanov, S.; Hristov, T. Mathematical and computer modeling of COVID-19 transmission dynamics in Bulgaria by time-depended inverse SEIR model. *AIP Conf. Proc.* **2021**, *2333*, 090024. [CrossRef]

Disclaimer/Publisher's Note: The statements, opinions and data contained in all publications are solely those of the individual author(s) and contributor(s) and not of MDPI and/or the editor(s). MDPI and/or the editor(s) disclaim responsibility for any injury to people or property resulting from any ideas, methods, instructions or products referred to in the content.